Energetically consistent Eddy-Diffusivity Mass-Flux schemes for Atmospheric and Oceanic Convection

Manolis Perrot, Florian Lemarié

Energetically consistent Eddy-Diffusivity Mass-Flux schemes for Atmospheric and Oceanic Convection

M. Perrot[1,*], **F. Lemarié**[1]

[1]Univ Grenoble Alpes, Inria, CNRS, Grenoble INP, LJK, Grenoble, France

Key Points:

- An Eddy-Diffusivity Mass-Flux parameterization is carefully derived from first principles, making the underlying assumptions explicit
- Closed energy budgets between resolved and subgrid energy reservoirs are outlined, including a new formulation of vertical TKE transport
- Comparisons with Large Eddy Simulations show that the new scheme successfully reproduces TKE and its vertical transport

Corresponding author: Manolis Perrot, `manolis.perrot@univ-grenoble-alpes.fr`

Abstract

This study aims to introduce a new convective vertical mixing scheme rooted in the Eddy-Diffusivity Mass-Flux (EDMF) approach, itself derived from first principles. The integration of the mass-flux (MF) concept with the Eddy-Diffusivity (ED) approach has long been studied and applied in global and regional atmospheric models for parameterizing convection, both dry and cloudy, and sees a growing interest in ocean models. This type of closure involves separating vertical turbulent fluxes into two components: a diffusion term that addresses local small-scale mixing in a near isotropic environment and a mass-flux transport term that accounts for the non-local transport due to vertically coherent plumes within the environment. Here, we exploit the multi-fluid averaging technique underlying the MF concept to propose an original formulation of a scheme that possesses properties not satisfied by most existing EDMF formulations. Consistent energy budgets between resolved and subgrid scales are derived for different multi-component fluids including seawater and dry atmosphere (in Boussinesq and anelastic cases). This guarantees that all mean kinetic, potential, and internal energy sinks and sources as long as turbulent kinetic energy (TKE) transport associated with EDMF terms are exactly added or subtracted to the TKE budget, effectively rectifying energy biases existing in prior EDMF schemes. Notably, this analysis facilitates a clear separation of convective and turbulent small-scale energy reservoirs. In addition to bulk energy transfers, we provide guidelines to avoid spurious energy fluxes at the fluid's boundary when using EDMF. We illustrate the performance of the proposed *energetically consistent EDMF scheme* in the context of oceanic convection. When compared with Large Eddy Simulations (LES) of oceanic convection, our scheme can reproduce mean fields as well as higher-order moments such as TKE, vertical fluxes, and turbulent transport of TKE. The energetic consistency is key to obtaining realistic TKE and turbulent transport of TKE profiles. To further illustrate that the MF concept is a credible alternative to the traditional approaches used in the oceanic context (using an enhanced vertical diffusion or a counter gradient term *à la* KPP) the proposed scheme is validated in a single-column configuration against observational data of oceanic convection from the LION buoy. Last but not least, during the theoretical development of the scheme, we maintain transparency regarding underlying assumptions and systematically assess their validity in the light of LES data.

Plain Language Summary

In Earth system models, various important processes occur on scales that are too fine to be resolved with usual grid resolutions. Parameterizations have to be used to approximate the average effect of such processes on the scales resolved by a numerical model. The general objective of the proposed work is to approach the parameterization problem for boundary-layer turbulence and convective plumes in a "consistent" manner. Here the notion of consistency integrates various aspects: global energetic consistency, consistency with a particular averaging technique for the scale-separation, and the rigorous reduction of a physical system to a scale-aware parametric representation based on well-identified and justifiable approximations and hypotheses. An originality is to jointly consider energy budgets including a subgrid energy reservoir on top of the resolved energies allowing the proper coupling between the parameterization and the resolved fluid dynamics. This research is fundamental to obtain an apt representation of mean fields and higher-order turbulent moments and to pave the way toward an alternative methodology to parameterize oceanic convection across scales. Numerical simulations demonstrate the adequacy of the proposed parameterization.

1 Introduction

1.1 Convection in the ocean and atmosphere and its parameterization in numerical models

Boundary layer convection occurs in the atmosphere and the ocean due to buoyancy fluxes at the surface, which trigger gravitational instabilities. Buoyant plumes then tend to overturn and mix the fluid. When looking at the mean properties of the fluid, it leads to the formation of a well-mixed layer. The accurate representation of such boundary layers is of paramount importance for short-term forecasts as well as for climate projections in the atmosphere (Bony et al., 2015; Schneider et al., 2017) and the ocean (Martin et al., 2013; Piron et al., 2016; Moore et al., 2015; Fox-Kemper et al., 2019). Regarding current computational capacities, plumes are still unresolved in regional and global numerical models, and thus their effects require parameterization. Moreover in ocean modeling, beyond the requirement in terms of grid resolution, hydrostatic equations used in the overwhelming majority of regional and global studies are not suitable for resolving convective phenomena explicitly (Marshall et al., 1997).

For any quantity X, standard turbulent mixing models are based on the closure of vertical turbulent fluxes $\overline{w'X'}$ proportional to the local mean gradient in the form $-K_X\partial_z\overline{X}$ (which corresponds to the so-called Eddy-Diffusivity (ED) closure). Such a closure leads to a diffusion of $\overline{X}$, which is often justified by considering that turbulent fluctuations resemble Brownian motion (Vallis, 2017; Resseguier et al., 2017). Although the ED closure has been widely used in many industrial and geophysical applications, it is known to potentially predict incorrectly higher order moments and even mean fields for complex flows (e.g. Schmitt, 2007). For instance, the inadequacy of ED closures for atmospheric convection has long been highlighted (Deardorff, 1966). Indeed fluctuations are carried by non-local structures, the buoyant plumes, that can be coherent over the whole mixed layer. In particular, in such a layer, mean gradients are close to zero ($\partial_z\overline{X} \simeq 0$) while transport is ensured at leading order by non-zero vertical fluxes $\overline{w'X'}$ which may even be up-gradient. Indeed, using the assumption of a mixed-layer $\partial_z\overline{X} \simeq 0$ into a turbulent transport equation of the type $\partial_t\overline{X} + \partial_z\overline{w'X'} = 0$ implies that $\overline{w'X'}$ varies linearly with z. Such linear variation of fluxes in the mixed layer is well-supported by observations and numerical experiments (Garratt, 1994b; Denbo & Skyllingstad, 1996).

To circumvent ED hypothesis, Deardorff (1966) proposed to introduce a constant non-local term γ_X in the form $\overline{w'X'} = -K_X(\partial_z\overline{X} - \gamma_X)$. Later on, such a formulation has been refined, where both K_X and γ_X were prescribed by a self-similar profile function depending on external characteristics of the boundary layer such as surface forcing, stratification at the atmospheric top (or oceanic base) of the mixed layer and implicitly defined mixed layer height (see Troen and Mahrt (1986); Holtslag and Moeng (1991) for atmospheric models, Large et al. (1994) for oceanic models). This approach is still in use in some present-day ocean models (e.g. via the CVMIX library, Van Roekel et al., 2018). Furthermore, in the context of ocean models, two other types of convective parameterization are sometimes used: (*i*) a buoyancy sorting scheme (a.k.a. adjustment scheme or non-penetrative scheme), in which static instabilities are eliminated in one time-step by mixing downward neighboring vertical levels until a neutral buoyancy profile is attained (e.g. Madec et al., 1991) (*ii*) an enhanced eddy-viscosity scheme in which the vertical diffusivity coefficient is artificially increased to a high value as soon as static instabilities are found on the density profiles. These two approaches are not grounded on a physical derivation.

The present work builds on the combined Eddy-Diffusivity and Mass-Flux (EDMF) parameterization schemes (Hourdin et al., 2002; Soares et al., 2004). The ED component aims to represent turbulent transport in a nearly isotropic environment, in which convective plumes -modeled by MF terms- support a non-local advective transport. The MF concept was originally introduced in the atmospheric context to represent deep con-

vective clouds (Arakawa & Schubert, 1974), then it has been adapted to represent shallow and dry boundary layer convection in combination with ED schemes. It is intrinsically based on a multi-fluid averaging (Yano, 2014; Thuburn et al., 2018) of the fluid equations. In ocean models the EDMF concept has been first introduced by Giordani et al. (2020), and has been gaining increasing attention (e.g. Garanaik et al. (2024), or a recent implementation in Oceananigans, Ramadhan et al. (2020)).

1.2 Parameterization development and physics dynamics coupling

The general objective of the proposed work is to approach the parameterization problem in a "consistent" manner. Here the notion of consistency integrates various aspects: consistency with the laws of physics, energetic consistency at both continuous (e.g. Eden, 2016; Jansen et al., 2019; Eden & Olbers, 2014) and discrete (e.g. Burchard, 2002) levels, consistency with a particular choice of scale-separation operator (Higgins et al., 2013; Lauritzen et al., 2022), and the rigorous reduction of a physical system to a scale-aware parametric representation based on well-identified approximations and hypotheses (Honnert et al., 2016; Tan et al., 2018).

Regarding boundary layer parameterizations, eddy-diffusivity intensity often scales with the turbulent kinetic energy (TKE) which is computed via a parameterized prognostic equation. TKE represents a subgrid kinetic energy that exchanges energy with the resolved reservoirs. The use of mass-flux terms leads to energy transfers and redistributions that must be taken into account in the TKE equation to ensure energetic consistency between resolved and subgrid scales. In addition, the boundary conditions of the mass-flux equations must be consistent between ED and MF to avoid double-counting and artificial energy fluxes at the fluid boundary. Apart from a brief discussion in Tan et al. (2018) for unsteady plume models, the energetically consistent coupling of TKE and standard EDMF schemes has not been, to our knowledge, discussed in the literature. Some modifications of the TKE equation when using a mass-flux model have been proposed for the buoyancy production term (Witek et al., 2011b) and the vertical turbulent transport of TKE (Witek et al., 2011a; Han & Bretherton, 2019). However, these studies are not motivated by considerations of energetic consistency.

1.3 Goals and organisation of the paper

The aim of this paper is two-fold. First, we intend to provide an introductory, self-contained, and pedagogical derivation of EDMF schemes starting from first principles, to guide consistency considerations. Second, we derive theoretical energy budgets and provide guidelines to obtain energetically consistent EDMF models. Consequently, this paper is intended to both the oceanographic community as a pedagogical introduction to EDMF, and the atmospheric community seeking to reduce energy biases in EDMF models. The paper is organized as follows. In section 2, we expose the derivation of an EDMF scheme from first principle, systematically discuss the successive assumptions at stake, provide closures according to state-of-the-art practice, and discuss consistent boundary conditions. In section 3, we recall the theoretical resolved and subgrid energy budgets of a horizontally averaged Boussinesq fluid without closures. In section 4, we expose the necessary modification of the parameterized turbulent kinetic energy (TKE) equation to obtain closed energy budgets when using EDMF. Furthermore, we derive vertically averaged energy budgets to reveal the role of boundary conditions on the energy fluxes. In section 5, we analyze the assumptions used in the derivation of the scheme in light of data from Large Eddy Simulation (LES) of idealized oceanic deep convection. Then we evaluate the energetically consistent EDMF scheme against such data, and against realistic data of oceanic deep convection events in the Mediterranean Sea. In appendices, we provide discretization details for interested model developers and energy budgets in the anelastic setting which are more commonly used by the atmospheric community.

2 Derivation of EDMF scheme

2.1 Formal derivation

We start from the unaveraged Navier-Stokes equations under the Boussinesq assumption in a cubic domain $L_x \times L_y \times H$:

$$\nabla \cdot \boldsymbol{u} = 0 \tag{1}$$

$$\partial_t \boldsymbol{u} = -\nabla \cdot (\boldsymbol{u} \otimes \boldsymbol{u}) - \frac{1}{\rho_0}\nabla p^\dagger + b\boldsymbol{e}_z + \nu\nabla^2 \boldsymbol{u} \tag{2}$$

$$\partial_t \phi = -\nabla \cdot (\phi \boldsymbol{u}) + S_\phi \tag{3}$$

$$b = b_{\text{eos}}(\phi) \tag{4}$$

where $\boldsymbol{u} = (u, v, w)$ denotes the velocity field in a local Cartesian frame of reference $(\boldsymbol{e}_x, \boldsymbol{e}_y, \boldsymbol{e}_z)$, z ranges from 0 to H in the atmosphere and $-H$ to 0 in the ocean, ρ_0 is a constant reference density, the pressure has been decomposed as $p = p_{\text{ref}}(z) + p^\dagger(x, y, z, t)$ with $\partial_z p_{\text{ref}} = -\rho_0 g$, b is the buoyancy acceleration, ϕ is any entropic variable describing each component of the fluid, S_ϕ is an additional source term (typically molecular diffusion). For instance, in the context of a dry atmosphere modeled as an ideal gas, a simple choice[1] would be $\phi = \theta$, where θ is the potential temperature, and $b_{\text{eos}}(\theta) = g(\theta - \theta_0)/\theta_0$. In the context of ocean dynamics, one would choose conservative temperature and salinity ($\phi = \theta, S$) and a linear equation of state, $b_{\text{eos}}(\theta, S) = g\alpha(\theta - \theta_0) - g\beta(S - S_0)$ where α and β are thermal expansion and haline contraction coefficients, respectively, and θ_0 and S_0 are reference temperature and salinity. Details on source terms S_ϕ are given in section 3. For the sake of simplicity, we do not include the Coriolis term in the present study. Since the Coriolis force is energetically-neutral it does not interfere with the derivations made throughout this paper. Next, we explicit the framework in which vertical mixing parameterizations are usually developed. We adopt a semi-discrete approach, where the *horizontal* fluid domain is divided into a $N_x \times N_y$ mesh. Each horizontal grid cell has length Δx_i and width Δy_j, and we denote (x_i, y_j) its center. Note that the time and vertical coordinates z are kept *continuous*. The spatial domain can be thought of $N_x \times N_y$ vertical columns stacked together. In a numerical model discretized on such a mesh, the computed variables would be interpreted in a finite volume approach (LeVeque, 2002). For any field $X = \boldsymbol{u}, \phi...$ one can define the following horizontal average and fluctuation

$$\overline{X}(x_i, y_j, z, t) := \frac{1}{\Delta x_i \Delta y_j} \int_{\Delta x_i \times \Delta y_j} X(x, y, z, t)\, \mathrm{d}x\mathrm{d}y, \qquad X' = X - \overline{X}$$

If we recast (1)–(3) in the generic form $\partial_t X + \nabla \cdot (\boldsymbol{u} X) = S_X$, and then apply such a horizontal average, we obtain

$$\partial_t \overline{X} + \partial_z \left(\overline{w}\overline{X} + \overline{w'X'} \right) + \frac{1}{\Delta x_i \Delta y_j} \oint_{\partial(\Delta x_i \times \Delta y_j)} X \boldsymbol{u}_h \cdot \mathrm{d}\boldsymbol{n} = \overline{S}_X \tag{5}$$

where $\boldsymbol{u}_h = (u, v, 0)$ denotes the horizontal velocity vector and $\mathrm{d}\boldsymbol{n}$ is an outward pointing line integral element, i.e. $\boldsymbol{u}_h \cdot \mathrm{d}\boldsymbol{n} = u\mathrm{d}y - v\mathrm{d}x$. The boundary integral in (5) is the total (resolved and subgrid) horizontal flux of X. In a numerical model, $\overline{X}$ would be interpreted as the resolved variable, X' would be an unresolved fluctuation, the precise form of the horizontal flux would depend on the numerical scheme (and possibly on parameterizations), and the vertical subgrid flux $\overline{w'X'}$ has to be closed by a parameterization. When focusing on the parameterization of vertical mixing processes, it is common to conceptually isolate one vertical column of fluid to work with a one-dimensional Single-Column

[1] In both oceanic and atmospheric context, we use simple thermodynamic descriptions allowing convection. Although these descriptions are inaccurate for real-world applications, they are sufficient to expose how to build energetically consistent EDMF parameterizations. Energy budgets for the anelastic approximation can be found in Appendix E

Model (SCM) (e.g. Zhang et al., 2016). Any quantity is assumed statistically invariant along the horizontal direction, meaning that in practice the horizontal fluxes and pressure gradients are neglected. We further simplify the problem with two additional assumptions: First, the bottom of the column is considered flat. Along with a non-penetration condition, this leads to $\overline{w}(z=0)=0$. Now the averaged volume conservation under the horizontal homogeneity $\partial_z\overline{w}=0$ implies that $\overline{w}(z)=0$ at any level z. Second, in the vertical momentum budget, the momentum flux divergence $\partial_z\overline{w'w'}$ is neglected, leading to the hydrostatic approximation $\partial_z\overline{p}^\dagger = b$. The SCM equations are then

$$\partial_t\overline{\boldsymbol{u}}_h = -\partial_z\overline{w'\boldsymbol{u}'_h} \tag{6}$$
$$\partial_t\overline{\phi} = -\partial_z\overline{w'\phi'} + \overline{S}_\phi \tag{7}$$

where the molecular viscosity can be safely neglected in the mean momentum budget. The remainder of this article will use these SCM assumptions, and indices i,j will be dropped. For readers interested in the inclusion of horizontal fluxes, we refer them to Yano (2014) and Tan et al. (2018). As an alternative to the semi-discrete description presented above, a fully continuous description can be carried out by replacing the horizontal average by smoothing kernels on the scale of the grid size (see for example Thuburn et al. (2018) in the context of mass-flux schemes).

We now *assume* a formal decomposition of the horizontal column area $\Delta x\times\Delta y$ into two horizontal subdomains of areas $\mathcal{A}_e(z,t)$ and $\mathcal{A}_p(z,t)$ which also depend on depth and time. Such decomposition is meant to isolate the coherent convective structures usually referred to as *plumes* (occupying the subdomain of area $\mathcal{A}_p(z,t)$) from the rest of the flow, referred to as the *environment* (occupying the subdomain of area $\mathcal{A}_e(z,t)$). We introduce the following notations to characterize the subdomain averaged field and *fractional* area (for $i=e,p$):

$$X_i = \frac{1}{\mathcal{A}_i(z,t)}\int_{\mathcal{A}_i(z,t)} X(x,y,z,t)\,\mathrm{d}x\mathrm{d}y$$
$$a_i = \mathcal{A}_i(z,t)/(\Delta x\times\Delta y)$$

Any mean field can then be decomposed as

$$\overline{X} = a_eX_e + a_pX_p$$

In particular, when $X\equiv 1$ we get the constraint $a_e = 1-a_p$. After some algebra, any turbulent flux can be recast as

$$\overline{w'X'} = a_e\overline{w'_eX'_e} + a_p\overline{w'_pX'_p} + a_e(w_e-\overline{w})(X_e-\overline{X}) + a_p(w_p-\overline{w})(X_p-\overline{X}) \tag{8}$$

where

$$\overline{w'_iX'_i} = \frac{1}{\mathcal{A}_i(z,t)}\int_{\mathcal{A}_i(z,t)}(X-X_i)(w-w_i)\,\mathrm{d}x\mathrm{d}y$$

For each subdomain, the $a_i(w_i-\overline{w})(X_i-\overline{X})$ terms in (8) account for the "mass-flux" (i.e. the contribution of coherent structures to the flux), whereas the $a_i\overline{w'_iX'_i}$ terms are a contribution from internal variability. Applying the subdomain average to any conservation law of the form $\partial_tX+\nabla\cdot(\boldsymbol{u}X)=S_X$ and using Reynolds transport theorem leads to (see appendix A of Tan et al. (2018) and Yano (2014) for full derivation)

$$\partial_t(a_iX_i) + \partial_z\left(a_iw_iX_i + a_i\overline{w'_iX'_i}\right) + \frac{1}{\mathcal{A}_i}\oint_{\partial\mathcal{A}_i} X\boldsymbol{u}_r\cdot\mathrm{d}\boldsymbol{n} = a_iS_{X,i} \tag{9}$$

where the relative horizontal boundary velocity is $\boldsymbol{u}_r = \boldsymbol{u}_h - \partial_t\boldsymbol{r}_b - w\partial_z\boldsymbol{r}_b$ and $\boldsymbol{r}_b = (x_b(z,t),y_b(z,t))$ is the position vector of boundary elements. The three terms that consitute $\boldsymbol{u}_r$ indicate that boundary fluxes can arise respectively due to horizontal velocity across the boundary, to (apparent) horizontal velocity of the boundary, or to vertical velocity if the boundary of the 3D plume is vertically tilted (i.e. $\partial_z\boldsymbol{r}_b\neq 0$).

2.2 Standard assumptions

2.2.1 Plume-Environment decomposition

The first standard assumption we have already made is to consider only two subdomains, the convective plume and the environment. This is justified since in convective situations the main contribution to the fluxes comes from the plumes. However, the framework is flexible enough to incorporate an arbitrary number of components. In particular, several studies of the atmospheric convective boundary layer (CBL) underline the importance of returning coherent structures around the plumes, often referred to as CBL downdrafts (Schmidt & Schumann, 1989; Couvreux et al., 2007; Brient et al., 2023).

2.2.2 Entrainment/Detrainment and Upstream approximation

Net fluid exchange at the horizontal boundary of the plume domain can be further decomposed into fluid *entrained* into the plume from the environment, and fluid *detrained* out of the plume into the environment, namely

$$\begin{aligned}\frac{1}{\mathcal{A}_p}\oint_{\partial\mathcal{A}_p}\boldsymbol{u}_r\cdot\mathrm{d}\boldsymbol{n} &= \frac{1}{\mathcal{A}_p}\oint_{\partial\mathcal{A}_p,\boldsymbol{u}_r>0}\boldsymbol{u}_r\cdot\mathrm{d}\boldsymbol{n}+\frac{1}{\mathcal{A}_p}\oint_{\partial\mathcal{A}_p,\boldsymbol{u}_r<0}\boldsymbol{u}_r\cdot\mathrm{d}\boldsymbol{n}\\ &= D-E\end{aligned}$$

where $E(>0)$ is called *entrainment rate* and $D(>0)$ is called *detrainment rate*. We further assume that the value of X at the boundary is either equal to the mean value in the environment when entrainment is occurring, or the mean value in the plume when detrainment is occurring. This is the so-called *upstream approximation*, formulated as[2]

$$\frac{1}{\mathcal{A}_p}\oint_{\partial\mathcal{A}_p}X\boldsymbol{u}_r\cdot\mathrm{d}\boldsymbol{n}=X_eE-X_pD \tag{10}$$

As a result of this approximation, the plume equation reads

$$\partial_t(a_pX_p)+\partial_z(a_pw_pX_p)=-\partial_z(a_p\overline{w_p'X_p'})+EX_e-DX_p+a_pS_{X,p} \tag{11}$$

In particular when $X\equiv 1$, we get the plume area conservation equation:

$$\partial_t a_p+\partial_z(a_pw_p)=E-D \tag{12}$$

2.2.3 Steady plume hypothesis

A common hypothesis is that the plume domain is in a quasi-steady regime, thus neglecting the temporal tendency compared to vertical advection. The relevance of this hypothesis is numerically tested using idealized cases in section 5.3. An *a priori* scaling estimation can also be performed. Introducing τ, h, and W the characteristic time, depth, and vertical velocity scales of the plume, the order of magnitude of the ratio between the temporal tendency and vertical advection can be estimated as follows

$$O\left(\frac{\partial_t(a_pX_p)}{\partial_z(a_pw_pX_p)}\right)=\frac{h/\tau}{W}\simeq\frac{w_{\mathrm{ent}}}{W} \tag{13}$$

where $w_{\mathrm{ent}}=\frac{d}{dt}h$ is the boundary layer vertical entrainment velocity. In the limit of free convection triggered by a surface buoyancy loss $B_0<0$ into a fluid of constant stratification N_0^2, the classical convective scalings $h\propto\sqrt{-B_0/N_0^2t}$ and $W=(-B_0h)^{1/3}$ (Turner, 1979; Deardorff, 1970) lead to

$$\frac{w_{\mathrm{ent}}}{W}\propto\frac{1}{(N_0t)^{2/3}} \tag{14}$$

[2] In the context of 3D models, the plume boundary $\partial\mathcal{A}_p$ can cross the horizontal boundary of the grid cell. The corresponding contribution to the integral can be interpreted as a resolved flux divergence across the grid cell, namely $\nabla_h\cdot(a_p\boldsymbol{u}_{h,p}X_p+a_p\overline{\boldsymbol{u}_{h,p}'X_p'})$ (see section 5.1 of Yano (2014)).

In a different context, that of the development of a shear-driven mixed layer forced by surface wind stress $\rho_0 u_*^2$, Kato and Phillips (1969) showed that $w_{\text{ent}}/u_* \propto u_*^2/N_0^2 h$. In such a layer $W \simeq u_*$, leading to a scaling similar to (14). These scalings suggest that as long as the surface forcings (represented here by u_* and B_0) are evolving slowly compared to $1/N_0$, the steady plume hypothesis remains valid. Under such a hypothesis, the plume equation for any field X now reads

$$\partial_z(a_p w_p X_p) = -\partial_z(a_p \overline{w_p' X_p'}) + E X_e - D X_p + a_p S_{X,p} \tag{15}$$

As a summary, we rewrite the coupled resolved/plume system in an advective form using area conservation and $\overline{X} = (1-a_p)X_e + a_p X_p$:

$$\partial_t \overline{X} = -\partial_z \overline{w' X'} + \overline{S}_X \tag{16}$$

$$\overline{w' X'} = \frac{1}{1-a_p} a_p w_p (X_p - \overline{X}) + (1-a_p)\overline{w_e' X_e'} + a_p \overline{w_p' X_p'} \tag{17}$$

$$a_p w_p \partial_z X_p = -\frac{1}{1-a_p} E (X_p - \overline{X}) - \partial_z(a_p \overline{w_p' X_p'}) + a_p S_{X,p} \tag{18}$$

Several authors have recently proposed to relax the steady plume hypothesis (Tan et al., 2018; Thuburn et al., 2018). However, the overwhelming majority of mass flux schemes implemented in realistic models considers a plume domain in a quasi-steady regime.

2.2.4 Small area limit

A last standard hypothesis is that the fractional area of the plume is *small* compared to that of the environment (see section 5.3 for a direct evaluation against LES). This generally means considering the formal limit $a_p \to 0$ and $a_e \to 1$ in the previous equations while keeping non-zero mass-flux $a_p w_p$ and source terms. Yano (2014) proposes to assume $a_p w_p = O(w_e)$ and $a_p S_{X,p} = O(S_{X,e})$ to retain an order one contribution of $a_p w_p (X_p - \overline{X})$ in (17), and to keep an order one contribution of advection and forcings in (18). In the small area limit, any environmental field X_e (except w_e) can be approximated by the mean field, the vertical turbulent flux (17) becomes

$$\overline{w' X'} = a_p w_p (X_p - \overline{X}) + \overline{w_e' X_e'} \tag{19}$$

and the plume equation (18) now reads

$$a_p w_p \partial_z X_p = -E(X_p - \overline{X}) + a_p S_{X,p} \tag{20}$$

In the remainder of this study, we will adopt such a small area limit. Noteworthy is the effort by some authors to relax this hypothesis to explore the "grey zone" of atmospheric turbulence or to devise scale-aware parameterization schemes when the grid is refined to the point where a_p is no longer small (Honnert et al., 2016; Tan et al., 2018). For the sake of completeness, we include in Appendix A the system of plume equations obtained when relaxing the small area limit while still neglecting subplume fluxes $\overline{w_p' X_p'}$ (in line with Tan et al. (2018)). This system only deviates by factors $1/(1-a_p)$ from the "small-area" system, making it simple to implement in practice.

Remark: To our knowledge, the interplay between the small area limit and the steady plume hypothesis has been only discussed in Yano (2014) where the author argues that the formal limit $a_p \to 0$ implies $\partial_t(a_e X_e) \to \partial_t \overline{X}$, and thus recovers the steady-plume hypothesis $\partial_t(a_p X_p) \to 0$ using (8). Using such formal limit and $a_p w_p = O(w_e)$ implies that $w_p \to \infty$. Since plume properties are advected by w_p, such infinite velocity assumption is interpreted as an instantaneous adjustment to any surface perturbation, consistently with the steady-plume hypothesis. Using Yano's scaling, an estimate of the ratio between temporal tendency and vertical advection is now

$$O\left(\frac{\partial_t(a_p X_p)}{\partial_z(a_p w_p X_p)}\right) = \frac{O(a_p)/\tau}{w_e/h} \to 0 \text{ if } a_p \to 0$$

which shows that such scaling indeed implies stationarity. However, the alternative scaling we proposed in (13) decouples the small area limit from the stationarity assumption and is found to be validated in numerical simulations (see 5.3). Moreover, our scaling analysis seems more general since it merely takes into account scales for each field, without further assumptions, and thus justifies the potential use of stationary equations while relaxing the small area assumption.

2.3 Standard Closures

Thanks to the assumptions made so far, we have arrived at equations of the general form (20) for the plume, and (19) for vertical turbulent fluxes. At this stage, additional closure assumptions are required to express the entrainment and detrainment rates, the flux $\overline{w'_e X'_e}$, and the pressure gradients appearing in the $S_{w,p}$ and $S_{\boldsymbol{u}_h,p}$ terms.

2.3.1 Plume vertical pressure gradient

Plume vertical pressure gradients are usually parameterized as the combination of a virtual mass term (e.g. Bretherton et al., 2004) – representing the reduction of plume buoyancy due to pushing and pulling on the environment –, a reduced entrainment term and a quadratic drag term. Several formulations have been proposed (see Roode et al. (2012) for an intercomparison in the context of shallow cumulus convection). In line with usual practices in the atmospheric context (e.g. Pergaud et al., 2009; Rio et al., 2010) we consider

$$a_p \left(\frac{1}{\rho_0} \partial_z p^\dagger \right)_p \quad = \quad (a-1) a_p B_p + (b-1)(-E w_p) + b' a_p w_p^2 \tag{21}$$

leading to the plume vertical momentum budget

$$a_p w_p \partial_z w_p \quad = \quad a a_p B_p - b E w_p - \sigma_o^a b' a_p w_p^2 \tag{22}$$

where a, b and b' are positive parameters, $\sigma_o^a = +1$ in the atmosphere and -1 in the ocean, and $B_p = b_p - \overline{b}$. Note that in the case of dry atmosphere or seawater with a linearized equation of state, we have $b_p - \overline{b} = b_{\rm eos}(\phi_p) - b_{\rm eos}(\overline{\phi})$.

2.3.2 Horizontal momentum budget

Based on the work of Rotunno and Klemp (1982) and Wu and Yanai (1994), Gregory et al. (1997) proposed a parameterization of the plume horizontal pressure gradient as an advective correction of the form

$$a_p \left(\frac{1}{\rho_0} \nabla_h p^\dagger \right)_p = a_p w_p C_u \partial_z \overline{\boldsymbol{u}}_h \tag{23}$$

where C_u is a parameter. We show in Section 4.5 that energy cosntraints impose $0 \leq C_u < 1$.

2.3.3 Eddy-Diffusivity closure

The environment is thought of as a subdomain where only small-scale turbulence occurs, thus supporting the hypothesis of a closure of the vertical flux with an eddy-diffusivity, $\overline{w'_e X'_e} \underset{\rm ED}{=} -K_X \partial_z X_e \underset{a_p \ll 1}{\simeq} -K_X \partial_z \overline{X}$. This leads to the eddy-diffusivity mass-flux closure of subgrid fluxes

$$\overline{w' X'} = \underbrace{-K_X \partial_z \overline{X}}_{\rm ED} + \underbrace{a_p w_p (X_p - \overline{X})}_{\rm MF} \tag{24}$$

In the present study, the eddy viscosity K_u and diffusivity K_ϕ in turbulent vertical fluxes are computed from a turbulence closure model based on a prognostic equation for the

turbulent kinetic energy (TKE) $k = \overline{\boldsymbol{u}' \cdot \boldsymbol{u}'}/2$ and a diagnostic computation of appropriate length scales (a.k.a. 1.5-order turbulence closure). For the numerical tests in the oceanic context presented in Sec. 5, we use a formulation close to that of the Nucleus for European Modelling of the Ocean model (NEMO, Madec et al., 2019). The eddy-viscosity and diffusivity are classically assumed to be related to TKE by

$$\begin{aligned} K_u &= c_m l_m \sqrt{k} \\ K_\phi &= K_u (\mathrm{Pr}_t)^{-1} \end{aligned}$$

with l_m a mixing length scale, Pr_t the non-dimensional turbulent Prandtl number, and c_m is a constant (further details on the computations of these quantities are given in Appendix B). Details of the prognostic equation for k, in connection with energetic consistency requirements, are given in Sec. 3. We acknowledge that since ED represents turbulence in the environment, one should use the environmental TKE $1/2\overline{\boldsymbol{u}'_e \cdot \boldsymbol{u}'_e}$ instead as it is done in Tan et al. (2018). Although no significant effect could be seen in preliminary idealized numerical tests, this point should be further explored.

2.3.4 Entrainment and detrainment closures

Entrainment and detrainment closures are still a topic of extensive research in the atmospheric modeling community. One difficulty is that a given closure can only be specific to a certain type of convection (de Rooy et al., 2013). To close entrainment and detrainment rates[3], we adapt the formulation proposed by Rio et al. (2010), namely

$$E = a_p \beta_1 \max(0, \partial_z w_p) \tag{25}$$

$$D = -a_p \beta_2 \min(0, \partial_z w_p) + \sigma_o^a a_p w_p \delta_0 \tag{26}$$

where the two parameters β_1 and β_2 are positive, δ_0 is a positive minimum detrainment. In order to guarantee $0 \leq a_p \leq 1$, it is sufficient to impose $0 \leq \beta_1 \leq 1$ and $1 \leq \beta_2 < 2$ (see Appendix F).

To summarize the formal derivation made so far, the closure of fluxes and associated plume equations of the resulting EDMF scheme are provided in Tab. 1.

2.4 Consistent boundary conditions for mean and plume equations

2.4.1 General concepts

Under the aforementioned assumptions, the budget equations governing plume quantities simplify into a system of non-linear first-order ordinary differential equations with respect to the variable z. Accordingly, a single boundary condition at $z = 0$ (i.e., the top of the water column or the bottom of the air column depending on the fluid under consideration) is sufficient for the computation of plume variables. At the boundary $z = 0$, consistent boundary conditions for the plume variable X_p and the mean variable $\overline{X}$ must comply with the EDMF flux decomposition (24)

$$\overline{w'X'}(0) = -K_X \partial_z \overline{X}(0) + a_p(0) w_p(0) (X_p(0) - \overline{X}(0)) \tag{27}$$

Such a constraint should guide modeling choices concerning boundary conditions. Indeed, it systematically guarantees the correct partition of surface fluxes, and thus avoids double-counting biases linked to non-physical energy sources/sinks at the boundary (see Sec. 4.5). For instance, suppose the values of $\overline{w'X'}(0)$, $a_p(0)$, $w_p(0)$ and $X_p(0)$ are jointly

[3] In the literature, closures are usually provided for *fractional* entrainment and detrainment rates, respectively $\epsilon = E/(\sigma_o^a a_p w_p)$ and $\delta = D/(\sigma_o^a a_p w_p)$, where $-a_p w_p$ is the oceanic mass-flux and $+a_p w_p$ is the atmospheric mass-flux.

$\overline{w'\phi'}$	$= a_p w_p(\phi_p - \overline{\phi}) - K_\phi \partial_z \overline{\phi}$	Vertical turbulent flux for component ϕ
$\overline{w'\boldsymbol{u}'_h}$	$= a_p w_p(\boldsymbol{u}_{h,p} - \overline{\boldsymbol{u}}_h) - K_u \partial_z \overline{\boldsymbol{u}}_h$	Vertical turbulent momentum flux
$\partial_z(a_p w_p)$	$= E - D$	Plume area conservation equation
$a_p w_p \partial_z \phi_p$	$= E(\overline{\phi} - \phi_p)$	Plume equation for component ϕ
$a_p w_p \partial_z \boldsymbol{u}_{h,p}$	$= E(\overline{\boldsymbol{u}}_h - \boldsymbol{u}_{h,p}) + a_p w_p C_u \partial_z \overline{\boldsymbol{u}}_h$	Plume horizontal momentum equation
$a_p w_p \partial_z w_p$	$= -bE w_p + a_p \left\{ a B_p - \sigma_o^a b'(w_p)^2 \right\}$	Plume vertical velocity equation
B_p	$= b_{\text{eos}}(\phi_p) - b_{\text{eos}}(\overline{\phi})$	Buoyancy forcing term
K_u	$= c_m l_m \sqrt{k}$	Eddy-viscosity
K_ϕ	$= K_u \left(\text{Pr}_t\right)^{-1}$	Eddy-diffusivity

Table 1: Summary of the vertical turbulent flux formulation and plume equations in the small area limit under the steady plume hypothesis detailed in sections 2.1, 2.2 and 2.3. The mean terms quantities $\overline{\boldsymbol{u}}_h$ and $\overline{\phi}$ are the prognostic variables of the model and the equation for k is given in Sec. 4 and in Tab. 2.

specified. Then (27) would turn into a Robin (a.k.a type 3) boundary condition for the $\overline{X}$ equation which arises naturally in advection-diffusion equations (e.g. Hahn and Özişik (2012), chapter 1-5). At the boundary $z = \sigma_o^a H$, a no-flux condition is imposed for the mean equation. For the specific case of oceanic convection reaching the ocean bottom, a possibility is to add a penalization term to ensure the condition $w_p(z = -H) = 0$.

2.4.2 Oceanic context

For oceanographic applications, we consider that a surface flux $\overline{w'X'}(0)$ is prescribed. The mass flux component becomes non-zero close to the surface as soon as the entrainment rate (25) is itself non-zero. In this case the conservation of volume reads

$$\partial_z(a_p w_p) = a_p w_p \left(\beta_1 \frac{1}{w_p} \partial_z w_p + \delta_0 \right)$$

which can be easily integrated vertically to obtain

$$a_p(z) w_p(z) = (a_p(0) w_p(0)) \left(e^{\delta_0 z} \left(\frac{w_p(z)}{w_p(0)} \right)^{\beta_1} \right)$$

As $\beta_1 < 1$, non-trivial solutions are obtained if and only if non-zero boundary values for a_p and w_p are chosen. In the remainder, we adopt the following simple choice,

$$X_p(0) = \overline{X}(0),\ a_p(0) = a_p^0,\ w_p(0) = w_p^0$$

where a_p^0 and w_p^0 are parameters. According to (27), it implies that all the surface flux is allocated in the ED component, as advocated by Tan et al. (2018). This particular choice of boundary condition is also motivated by the fact that it implies at the discrete level that convection is triggered as soon as the surface Brünt-Väisälä frequency $\partial_z b(0)$ is negative (see Appendix F for further details). As a result, (27) turns into the Neumann boundary condition $-K_X \partial_z X(0) = \overline{w'X'}(0)$, which is standard practice for ED-only closures.

Alternatively, Soares et al. (2004) proposed that close to the surface, the plume/mean buoyancy difference B_p should depend on the surface buoyancy flux, leading to

$$b_p(z) = \overline{b}(z) + \beta \frac{\overline{w'b'}(0)}{\sqrt{k}(z)} \tag{28}$$

where β is a constant. We show in Appendix C that our formulation is in fact equivalent to (28) for if $\beta = z/(c_b l_b(0))$ and $k(z) \simeq k(0)$. However, when using this type of boundary condition exactly at the surface (as in Pergaud et al., 2009), special attention must be paid when providing the ED flux, since the EDMF decomposition (27) imposes

$$-K_b(0)\partial_z\overline{b}(0) = \left(1 - \frac{a_p(0)w_p(0)\beta}{\sqrt{k(0)}}\right)\overline{w'b'}(0)$$

which is different from the standard Neumann condition used for ED-only closures.

2.4.3 Atmospheric context: consistency with Monin-Obukhov theory

For atmospheric applications, boundary conditions for the mean variables are commonly imposed using Monin-Obukhov similarity theory (MOST), which assumes that in a surface layer located between $z = 0$ and $z = z_1$ fluxes are constant, and mean variables obey a quasi-logarithmic profile. To properly include a surface layer obeying MOST, then the EDMF flux decomposition must be imposed at the new model boundary $z = z_1$, namely

$$\overline{w'X'}(z_1) = -K_X(z_1)\partial_z\overline{X}(z_1) + a_p(z_1)w_p(z_1)(X_p(z_1) - \overline{X}(z_1)) \tag{29}$$

At this stage, we can point the following ambiguity. When the MF term is non-zero, it is not clear whether the flux arising from MOST – which is an ED flux – should be allocated to the ED term $-K_X(z_1)\partial_z\overline{X}(z_1)$, or to the total flux $\overline{w'X'}(z_1)$ using the constant flux assumption. Although not discussed transparently, it seems that the second option is a common practice. However, in such a case, special attention would be required to compute the total flux entering in energy budget computations.
Although beyond the scope of this article, we would like to point out that MOST is known to fail in strongly unstable conditions (Johansson et al., 2001; Li et al., 2018). Recently, Li et al. (2021) proposed corrections to formulate departure from MOST in the form of an EDMF closure including updraft *and* downdraft contributions. This approach could potentially help provide physically consistent boundary conditions to EDMF models.

At this stage, we have provided all the elements and underlying assumptions required to formulate an EDMF-type scheme (see Appendix F for the discretization aspects). Before studying the energetic impacts of using MF components, we derive theoretical horizontally averaged energy budgets.

3 Horizontally Averaged Energy budgets

The total specific energy E_{tot} of the fluid is the sum of the mean kinetic energy $E_k = (\overline{\boldsymbol{u}}_h \cdot \overline{\boldsymbol{u}}_h)/2$, the turbulent kinetic energy $k = (\overline{\boldsymbol{u}' \cdot \boldsymbol{u}'})/2$, the potential energy $E_p = gz$ and the mean internal energy E_i. In the following sections, we recall the expression of these energy reservoirs under the Boussinesq approximation, and we derive budgets for each of these reservoirs, regarless of flux parameterization. For completeness, energy budgets for anelastic models of dry atmosphere are derived in Appendix E.

3.1 Kinetic energies

Under the SCM assumptions exposed in Sec. 2.1, we can derive budgets for the resolved kinetic energy E_k and the turbulent kinetic energy k:

$$\partial_t E_k + \partial_z T_{E_k} = \overline{w'\boldsymbol{u}'_h} \cdot \partial_z \overline{\boldsymbol{u}}_h \tag{30}$$

$$\partial_t k + \partial_z T_k = -\overline{w'\boldsymbol{u}'_h} \cdot \partial_z \overline{\boldsymbol{u}}_h + \overline{w'b'} - \overline{\epsilon}_\nu \tag{31}$$

where $\overline{\epsilon}_\nu = \nu\overline{\partial_z \boldsymbol{u}' \cdot \partial_z \boldsymbol{u}'}$ is the viscous dissipation of energy, whereas $T_{E_k} = \overline{w'\boldsymbol{u}'_h} \cdot \overline{\boldsymbol{u}}_h$ and $T_k = \overline{w'\frac{\boldsymbol{u}'\cdot\boldsymbol{u}'}{2}} + \frac{1}{\rho_0}\overline{w'p^{\dagger\prime}} - \nu\partial_z k$ resdistribute energy on the vertical. Exchanges between the resolved and subgrid reservoirs of kinetic energy are done via the mechanical

shear term $\overline{w'\boldsymbol{u}_h'}\cdot\partial_z\overline{\boldsymbol{u}}_h$. To close the budgets, we provide in the following sections a budget for internal and potential energy.

3.2 Internal and Potential energies

For a generic fluid, the unaveraged specific internal energy can be written as

$$\mathcal{E}_i = \hbar(p,\phi) - \frac{p}{\rho} \tag{32}$$

where $\hbar$ is the specific enthalpy and ϕ is any entropic variable describing components of the fluid. Under the Boussinesq approximation, internal energy is (Tailleux & Dubos, 2023)

$$\mathcal{E}_i = \hbar(p_0,\phi) + (p_{\rm ref}-p_0)\partial_p\hbar(p_0,\phi) - \frac{p_{\rm ref}}{\rho_0} \tag{33}$$

where we recall that $p_{\rm ref}(z) = -\rho_0 g z + p_0$, and the specific volume is by definition $1/\rho := \partial_p\hbar$. In particular, this implies that under the Boussinesq approximation $b(\phi) := -g(\rho(p_0,\phi)-\rho_0)/\rho(p_0,\phi)$ (e.g. sec. 3.4 of Eldred & Gay-Balmaz, 2021). The sum of unaveraged internal and potential energies can then be written as

$$\mathcal{E}_i + E_p = z(g-b) + \hbar(p_0,\phi) - \frac{p_0}{\rho_0} \tag{34}$$

which leads to the unaveraged budget (Young, 2010; Tailleux, 2012)

$$\partial_t(\mathcal{E}_i + E_p) + \nabla\cdot([(\hbar(p_0,\phi)+gz]\,\boldsymbol{u}) = \epsilon_\nu - wb \tag{35}$$

Upon averaging and using the SCM assumptions, the budget of mean internal energy $E_i = \overline{\mathcal{E}}_i$ and potential energy reads

$$\partial_t(E_i+E_p) + \partial_z(\overline{\partial_\phi\hbar_0}\,\overline{w'\phi'}) = \overline{\epsilon}_\nu - \partial_z(\overline{\phi}\,\overline{w'\partial_\phi\hbar_0'} + \overline{\phi' w'\partial_\phi\hbar_0'}) - \overline{w'b'} \tag{36}$$

where we introduced the notation $\hbar_0(\phi) := \hbar(p_0,\phi)$. Remark that if $\hbar(p_0,\phi)$ is linear in ϕ, we have closed relations $\overline{\hbar(p_0,\phi)} = \hbar(p_0,\overline{\phi})$ and $\overline{b(\phi)} = b(\overline{\phi})$.

As a summary, the budgets of mean kinetic energy, turbulent kinetic energy and the sum of mean internal and potential energy are

$$\begin{cases} \partial_t E_k + \partial_z T_{E_k} & = \overline{w'\boldsymbol{u}_h'}\cdot\partial_z\overline{\boldsymbol{u}}_h \\ \partial_t k + \partial_z T_k & = -\overline{w'\boldsymbol{u}_h'}\cdot\partial_z\overline{\boldsymbol{u}}_h + \overline{w'b'} - \overline{\epsilon}_\nu \\ \partial_t(E_i+E_p) + \partial_z(\overline{\partial_\phi\hbar_0}\,\overline{w'\phi'}) & = -\partial_z(\overline{\phi}\,\overline{w'\partial_\phi\hbar_0'} + \overline{\phi' w'\partial_\phi\hbar_0'}) - \overline{w'b'} + \overline{\epsilon}_\nu \end{cases} \tag{37}$$

where conversion of E_k into k occurs via mean shear, conversion of k into E_i occurs via viscous dissipation, and conversion of k into E_i+E_p occurs via buoyancy fluxes.

In the following, we illustrate these budgets for dry atmosphere and seawater.

3.2.1 Dry atmosphere

The specific enthalpy for a dry atmosphere modeled as an ideal gas $p = \rho R_d T$ is

$$\hbar(p,\theta) = c_p\left(\frac{p}{p_0}\right)^{R_d/c_p}\theta \tag{38}$$

which is linear in the potential temperature $\theta = T\,(p/p_0)^{-R_d/c_p}$. Using (33) the sum of mean internal and potential energy within the Boussinesq approximation is

$$E_i + E_p = \left(c_p - \frac{gz}{\theta_0}\right)\overline{\theta} + 2gz - \frac{p_0}{\rho_0} \tag{39}$$

and buoyancy is $b(\overline{\theta}) = g(\overline{\theta} - \theta_0)/\theta_0$. The budget of $E_i + E_p$ is

$$\partial_t(E_i + E_p) = \left(c_p - \frac{gz}{\theta_0}\right)\partial_t\overline{\theta} = \overline{\epsilon}_\nu - \partial_z\left(c_p\frac{\theta_0}{g}\overline{w'b'}\right) - \overline{w'b'} \tag{40}$$

where $\overline{w'b'} = \frac{g}{\theta_0}\overline{w'\theta'}$. As a summary, the budgets of mean kinetic energy, turbulent kinetic energy and the sum of mean internal and potential energy for a *dry atmosphere* within the Boussinesq approximation are

$$\begin{cases} \partial_t E_k + \partial_z T_{E_k} & = \overline{w'\boldsymbol{u}'_h}\cdot\partial_z\overline{\boldsymbol{u}}_h \\ \partial_t k + \partial_z T_k & = -\overline{w'\boldsymbol{u}'_h}\cdot\partial_z\overline{\boldsymbol{u}}_h + \frac{g}{\theta_0}\overline{w'\theta'} - \overline{\epsilon}_\nu \\ \left(c_p - \frac{gz}{\theta_0}\right)\partial_t\overline{\theta} + -\partial_z\left(c_p\overline{w'\theta'}\right) & = -\frac{g}{\theta_0}\overline{w'\theta'} + \overline{\epsilon}_\nu \end{cases} \tag{41}$$

3.2.2 Seawater with linearized equation of state

For an ocean with a linearized equation of state, Boussinesq buoyancy is

$$b(\theta, S) = g\alpha(\theta - \theta_0) - g\beta(\theta - S_0) \tag{42}$$

and specific enthalpy is

$$\hbar(p_0, \theta, S) = c_p\theta - gz(1 + \alpha(\theta - \theta_0) - \beta(\theta - S_0)) \tag{43}$$

Using (33), the budget of mean internal and potential energy is

$$\partial_t\left(c_p\overline{\theta} - z\overline{b}\right) = \overline{\epsilon}_\nu - \partial_z\left(c_p\overline{w'\theta'} - z\overline{w'b'}\right) - \overline{w'b'} \tag{44}$$

The budgets of mean kinetic energy, turbulent kinetic energy, and the sum of mean internal and potential energy for *seawater* with a linearized equation of state are

$$\begin{cases} \partial_t E_k + \partial_z T_{E_k} & = \overline{w'\boldsymbol{u}'_h}\cdot\partial_z\overline{\boldsymbol{u}}_h \\ \partial_t k + \partial_z T_k & = -\overline{w'\boldsymbol{u}'_h}\cdot\partial_z\overline{\boldsymbol{u}}_h + \overline{w'b'} - \overline{\epsilon}_\nu \\ \partial_t\left(c_p\overline{\theta} - z\overline{b}\right) + \partial_z T_{E_i+E_p} & = -\overline{w'b'} + \overline{\epsilon}_\nu \end{cases} \tag{45}$$

Using the salt budget $\partial_t\overline{S} = -\partial_z\overline{w'S'}$, we can split this last equation as

$$\partial_t\overline{\theta} = \frac{\overline{\epsilon}_\nu}{c_p - \alpha gz} - \partial_z\overline{w'\theta'} \tag{46}$$

$$\partial_t(-z\overline{b}) = -zg\alpha\frac{\overline{\epsilon}_\nu}{c_p - \alpha gz} + \partial_z(z\overline{w'b'}) - \overline{w'b'} \tag{47}$$

Since the energy increase due to viscous dissipation is negligible in the ocean, $-z\overline{b}$ is often used as a proxy for "potential" energy (e.g. McDougall, 2003; Olbers et al., 2012). We nevertheless retain this dissipative heating in (46) to work with a properly closed energy budget in theoretical descriptions.

4 Consistency of TKE equation with EDMF closures

Based on the energy budgets described in the previous section, we provide a new parameterization of the TKE budget to obtain an energetically consistent model mimicking (37). Indeed, the following TKE equation is commonly used in TKE-based numerical models regardless of whether ED or EDMF closure is used,

$$\partial_t k + \partial_z(-K_k\partial_z k) = K_u\partial_z\overline{\boldsymbol{u}}_h\cdot\partial_z\overline{\boldsymbol{u}}_h - K_\phi\partial_z\overline{b} - \overline{\epsilon}_\nu \tag{48}$$

where k represents the turbulent kinetic of the whole grid cell, *i.e.* $1/2\overline{\boldsymbol{u}'\cdot\boldsymbol{u}'}$. In (48), turbulent fluxes have been closed using ED. However, we argue that if an EDMF closure is used in the mean equations (for momentum, temperature, and salinity or humidity), the TKE equation should be modified by MF terms to ensure energetic consistency as shown below. Note that Tan et al. (2018) made a different choice by considering a budget for the *environmental* TKE, $k_e = 1/2\overline{\boldsymbol{u}'_e\cdot\boldsymbol{u}'_e}$.

4.1 Shear and Buoyancy terms

We have seen in (37) that sources of turbulent kinetic energy could arise from the mean kinetic energy via mean shear $-\overline{w'\boldsymbol{u}'_h}\cdot\partial_z\overline{\boldsymbol{u}}_h$, or from internal and potential energies via buoyancy production $\overline{w'b'}$.

When the EDMF approach is used to close fluxes in the diagnostic equations of $\overline{\boldsymbol{u}}_h$ and $\overline{\phi}$, then the same closures must be used in turbulent kinetic energy budget to ensure energetic consistency. As a consequence, the shear term must be closed as

$$-\overline{w'\boldsymbol{u}'_h}\cdot\partial_z\overline{\boldsymbol{u}}_h \underset{\text{EDMF}}{=} -\left[-K_u\partial_z\overline{\boldsymbol{u}}_h + a_p w_p(\boldsymbol{u}_{h,p}-\overline{\boldsymbol{u}}_h)\right]\cdot\partial_z\overline{\boldsymbol{u}}_h \tag{49}$$

In the case of *dry atmosphere*, the buoyancy production term is

$$\overline{w'b'} \underset{\text{EDMF}}{=} \frac{g}{\theta_0}\left[-K_\theta\partial_z\overline{\theta} + a_p w_p(\theta_p-\overline{\theta})\right] \tag{50}$$

whereas in the case of *seawater* with linearized equation of state and $K_\phi = K_\theta = K_S$,

$$\begin{aligned}\overline{w'b'} &\underset{\text{EDMF}}{=} g\alpha\left[-K_\theta\partial_z\overline{\theta} + a_p w_p(\theta_p-\overline{\theta})\right] - g\beta\left[-K_S\partial_z\overline{S} + a_p w_p(S_p-\overline{S})\right]\\ &= -K_\phi\partial_z\overline{b} + a_p w_p(b_p-\overline{b})\end{aligned}$$

4.2 Fluxes of TKE

The redistribution terms of TKE are often little discussed in turbulence parameterization since they do not contribute directly to the vertically integrated energy budgets. However, they are of great importance in convective conditions where non-local transport dominates (Witek et al., 2011a). For instance, in the atmosphere, the TKE produced close to the surface due to destabilizing buoyancy fluxes is then transported by coherent plumes in the mixed layer. Taking into account MF transport of TKE is thus essential to achieve local energetic consistency, and model accurately TKE at any level z.

Turbulent fluxes of TKE arise from the contribution of a TKE transport term, a pressure redistribution term and a viscous flux,

$$T_k = \frac{1}{2}\overline{w'\boldsymbol{u}'\cdot\boldsymbol{u}'} + \frac{1}{\rho_0}\overline{w'p'} - \nu\partial_z k \tag{51}$$

For atmospheric and oceanic flow, the viscous flux is negligibly small and will be omitted. We will assume the pressure redistribution term to be small compared to the transport of TKE, as it is usually done in CBL schemes (e.g. Mellor, 1973). In numerical models, TKE transport is usually parameterized via K-diffusion, namely

$$\partial_z\left(\overline{w'\frac{\boldsymbol{u}'\cdot\boldsymbol{u}'}{2}}\right) \simeq -\partial_z(K_k\partial_z k) \tag{52}$$

However, within the framework exposed in section 2.1, we can apply the two-domain decomposition of the horizontal average to get the exact relation

$$\begin{aligned}\overline{w'\frac{\boldsymbol{u}'\cdot\boldsymbol{u}'}{2}} = \sum_{i=e,p}&\underbrace{a_i\frac{1}{2}\overline{\boldsymbol{u}'_i\cdot\boldsymbol{u}'_i w'_i}}_{\mathrm{I}_i} + \underbrace{a_i(\boldsymbol{u}_i-\overline{\boldsymbol{u}})\cdot\overline{\boldsymbol{u}'_i w'_i}}_{\mathrm{II}_i}\\ &+\underbrace{a_i(w_i-\overline{w})\frac{1}{2}\overline{\boldsymbol{u}'_i\cdot\boldsymbol{u}'_i}}_{\mathrm{III}_i} + \underbrace{a_i\frac{1}{2}(\boldsymbol{u}_i-\overline{\boldsymbol{u}})^2(w_i-\overline{w})}_{\mathrm{IV}_i}\end{aligned} \tag{53}$$

where: I_i is an intra-subdomain turbulent TKE transport; II_i is a transport of Reynolds stress by the coherent velocities; III_i is a transport of subdomain TKE by the coherent velocities (*i.e.* transport of TKE by mass-flux); IV_i is a transport of convective kinetic

energy by coherent velocities. Based on LES simulations (see Sec. 5.3), we found that: (*i*) I_p can be neglected, consistently with the small area limit; (*ii*) II_e and II_p are almost compensating, thus the sum $\mathrm{II}_e + \mathrm{II}_p$ can be neglected. Using $a_p w_p = -a_e w_e$, we can conveniently reformulate the remaining terms:

$$\mathrm{III}_e + \mathrm{III}_p + \mathrm{IV}_e + \mathrm{IV}_p = a_p w_p \frac{1}{1-a_p}\left(k_p + \frac{1}{2}\|\boldsymbol{u}_p - \overline{\boldsymbol{u}}\|^2 - k\right) \tag{54}$$

where we have used the following exact decomposition of TKE:

$$k = \frac{1}{2}a_e\|\boldsymbol{u}_e - \overline{\boldsymbol{u}}\|^2 + a_e k_e + \frac{1}{2}a_p\|\boldsymbol{u}_p - \overline{\boldsymbol{u}}\|^2 + a_p k_p \tag{55}$$

and $k_i := 1/2\overline{\boldsymbol{u}_i' \cdot \boldsymbol{u}_i'}$ $(i = e, p)$. In EDMF closures, turbulence is assumed isotropic in the environment, thus we close $\frac{1}{2}\overline{\boldsymbol{u}_e' \cdot \boldsymbol{u}_e' w_e'}$ with K-diffusion, similar to the standard practice for TKE-only schemes. Then assuming $\frac{1}{1-a_p} \simeq 1$ (i.e. the small area limit) we have

$$\overline{w'\frac{\boldsymbol{u}' \cdot \boldsymbol{u}'}{2}} \simeq \underbrace{-K_k \partial_z k}_{\mathrm{ED}} + \underbrace{a_p w_p \left(k_p - k + \frac{1}{2}\|\boldsymbol{u}_p - \overline{\boldsymbol{u}}\|^2\right)}_{\mathrm{MF}} \tag{56}$$

It is interesting to note that we can recover existing formulations from the proposed closure (56): if $a_p w_p = 0$ it boils down to the classical eddy-diffusivity closure; if $k_p = k$ and $\boldsymbol{u}_{h,p} = \overline{\boldsymbol{u}}_h$ the term $1/2 w_p^3$ proposed by Witek et al. (2011a) is recovered; if $\boldsymbol{u}_p = \overline{\boldsymbol{u}}$ then the formulation proposed by Han and Bretherton (2019) is recovered. However, we should mention that the latter authors treat TKE as a tracer to include the term $a_p w_p(k_p - k)$. This justification is incorrect because $\overline{w'\boldsymbol{u}' \cdot \boldsymbol{u}'/2}$ is not a second-order moment, but a third-order moment which requires a proper treatment as seen in (53).

Finally, one still needs to provide a value for k_p. Without any assumption, its prognostic equation reads (Tan et al., 2018, eq. (11))

$$\begin{aligned}
\partial_t(a_p k_p) + \partial_z(a_p w_p k_p) \quad = \quad & -a_p \overline{w_p' \boldsymbol{u}_{h,p}'} \cdot \partial_z \boldsymbol{u}_{h,p} + a_p \overline{w_p' b_p'} \\
& + E\left(k_e + \frac{1}{2}\|\boldsymbol{u}_e - \boldsymbol{u}_p\|^2\right) - D k_p \\
& - \partial_z\left(a_p \overline{w_p' \frac{\boldsymbol{u}_p' \cdot \boldsymbol{u}_p'}{2}} + a_p \overline{\boldsymbol{u}_p' \cdot \frac{1}{\rho_0}(\nabla p^\dagger)_p'}\right) \\
& - a_p(\epsilon_\nu)_p
\end{aligned}$$

As a first attempt, we propose to retain advection, entrainment, detrainment and dissipation terms, which lead to the simplified form of the previous equation:

$$\partial_z(a_p w_p k_p) \quad = \quad E\left(k_e + \frac{1}{2}\|\boldsymbol{u}_e - \boldsymbol{u}_p\|^2\right) - D k_p - a_p(\epsilon_\nu)_p \tag{57}$$

$$\quad = \quad E\left(\frac{1}{1-a_p}k - \frac{a_p}{1-a_p}k_p + \frac{1}{1-a_p}\frac{1}{2}(\boldsymbol{u}_p - \overline{\boldsymbol{u}})^2\right) - D k_p - a_p(\epsilon_\nu)_p \tag{58}$$

where we have used the identity $(\boldsymbol{u}_e - \boldsymbol{u}_p)^2 = \frac{1}{(1-a_p)^2}(\boldsymbol{u}_p - \overline{\boldsymbol{u}})^2$ and substituted k_e using (55). Using area conservation, we get the advective form

$$a_p w_p \partial_z k_p \quad = \quad E\frac{1}{1-a_p}\left(k - k_p + \frac{1}{2}(\boldsymbol{u}_p - \overline{\boldsymbol{u}})^2\right) - a_p(\epsilon_\nu)_p \tag{59}$$

Finally assuming $\frac{1}{1-a_p} \simeq 1$ (i.e. the small area limit) we have

$$a_p w_p \partial_z k_p \quad = \quad E\left(k - k_p + \frac{1}{2}(\boldsymbol{u}_p - \overline{\boldsymbol{u}})^2\right) - a_p(\epsilon_\nu)_p \tag{60}$$

As a summary, the proposed closure of TKE transport is given by

$$\overline{w' \frac{\boldsymbol{u}' \cdot \boldsymbol{u}'}{2}} = -K_k \partial_z k + a_p w_p \left(k_p - k + \frac{1}{2} \|\boldsymbol{u}_p - \overline{\boldsymbol{u}}\|^2 \right) \tag{61}$$

$$a_p w_p \partial_z k_p = E \left(k - k_p + \frac{1}{2} (\boldsymbol{u}_p - \overline{\boldsymbol{u}})^2 \right) - a_p (\epsilon_\nu)_p \tag{62}$$

4.3 Viscous dissipation

The total viscous dissipation rate is often parameterized as $\bar{\epsilon}_\nu = \frac{c_\epsilon}{l_\epsilon} k^{3/2}$ in standard ED schemes, we do the same for the plume viscous dissipation rate

$$(\epsilon_\nu)_p = \frac{c_\epsilon}{l_\epsilon} k_p^{3/2}$$

where $c_\epsilon = \sqrt{2}/2$ is a numerical constant and the dissipation length is $l_\epsilon = \sqrt{l_{\text{up}} l_{\text{dwn}}}$ (e.g. Gaspar et al., 1990) with l_{up} and l_{dwn} defined in Appendix B.

4.4 Boundary conditions

In general, providing physically relevant boundary conditions for the TKE equation is a complex question that we do not intend to answer in this study. However, once modelling choices are made, we can provide guidelines to utilize such boundary condition consistently within an EDMF scheme.

4.4.1 Generic constraint

According to (61), the boundary condition should verify at $z = 0$

$$\overline{w' \frac{\boldsymbol{u}' \cdot \boldsymbol{u}'}{2}} = -K_k \partial_z k + a_p w_p \left(k_p - k + \frac{1}{2} \|\boldsymbol{u}_p - \overline{\boldsymbol{u}}\|^2 \right) \tag{63}$$

In general if plume variables are specified at $z = 0$, then (63) is again a Robin boundary condition for the TKE equation.

4.4.2 Oceanic context

In the ocean, we will assume the following boundary conditions,

$$\overline{w' \frac{\boldsymbol{u}' \cdot \boldsymbol{u}'}{2}} = 0, \qquad k_p(0) = k(0)$$

along with $\boldsymbol{u}_p(0) = (\overline{u}(0), \overline{v}(0), w_p^0)$. In this case, (63) implies the following Neumann condition for TKE,

$$K_k \partial_z k(0) = \frac{1}{2} a_p^0 (w_p^0)^3 \tag{64}$$

Our formulation could handily include non-zero TKE flux at the surface, as proposed in the presence of wave-breaking (Craig & Banner, 1994; Mellor & Blumberg, 2004).

4.4.3 Atmospheric context

In atmospheric models, a value of TKE depending on friction and convective velocities is usually imposed at or near the surface, following field measurements of Wyngaard and Coté (1971). As long as the plume contribution to the surface TKE flux is imposed to be zero, the previous approach can be still used. If not, special care would have to be taken to enforce (63) and avoid spurious energy fluxes.

4.5 EDMF-parameterized budgets

Within the Boussinesq approximation, the budget of resolved kinetic energy, subgrid kinetic energy, and resolved internal+potential energy for a *dry atmosphere* with EDMF closure is

$$\begin{cases} \partial_t E_k + \partial_z T_{E_k} & = -K_u(\partial_z \overline{\boldsymbol{u}}_h)^2 + a_p w_p(\boldsymbol{u}_{h,p} - \overline{\boldsymbol{u}}_h)\cdot\partial_z\overline{\boldsymbol{u}}_h \\ \partial_t k + \partial_z T_k & = \frac{g}{\theta_0}\left[-K_\theta \partial_z\overline{\theta} + a_p w_p(\theta_p - \overline{\theta})\right] + K_u(\partial_z\overline{\boldsymbol{u}}_h)^2 - a_p w_p(\boldsymbol{u}_{h,p} - \overline{\boldsymbol{u}}_h)\cdot\partial_z\overline{\boldsymbol{u}}_h - \overline{\epsilon}_\nu \\ \partial_t\left[\left(c_p - \frac{gz}{\theta_0}\right)\overline{\theta}\right] + \partial_z T_{E_i+E_p} & = -\frac{g}{\theta_0}\left[-K_\theta\partial_z\overline{\theta} + a_p w_p(\theta_p - \overline{\theta})\right] + \overline{\epsilon}_\nu \end{cases} \tag{65}$$

where the flux terms are

$$T_{E_k} = (-K_u\partial_z\overline{\boldsymbol{u}}_h + a_p w_p(\boldsymbol{u}_{h,p} - \overline{\boldsymbol{u}}_h))\cdot\overline{\boldsymbol{u}}_h \tag{66}$$

$$T_k = -K_k\partial_z k + a_p w_p\left(k_p - k + \frac{1}{2}\|\boldsymbol{u}_p - \overline{\boldsymbol{u}}\|^2\right) \tag{67}$$

$$T_{E_i+E_p} = -c_p K_\theta\partial_z\overline{\theta} + c_p a_p w_p(\theta_p - \overline{\theta}) \tag{68}$$

Equivalently, in the case of *seawater* with linearized equation of state

$$\begin{cases} \partial_t E_k + \partial_z T_{E_k} & = -K_u(\partial_z\overline{\boldsymbol{u}}_h)^2 + a_p w_p(\boldsymbol{u}_{h,p} - \overline{\boldsymbol{u}}_h)\cdot\partial_z\overline{\boldsymbol{u}}_h \\ \partial_t k + \partial_z T_k & = -K_\phi\partial_z\overline{b} + a_p w_p(b_p - \overline{b}) + K_u(\partial_z\overline{\boldsymbol{u}}_h)^2 - a_p w_p(\boldsymbol{u}_{h,p} - \overline{\boldsymbol{u}}_h)\cdot\partial_z\overline{\boldsymbol{u}}_h - \overline{\epsilon}_\nu \\ \partial_t\left(c_p\overline{\theta} - z\overline{b}\right) + \partial_z T_{E_i+E_p} & = -\left(-K_\phi\partial_z\overline{b} + a_p w_p(b_p - \overline{b})\right) + \overline{\epsilon}_\nu \end{cases} \tag{69}$$

where the flux of internal and potential energy is

$$T_{E_i+E_p} = -\partial_z\left(c_p\left(-K_\phi\partial_z\overline{\theta} + a_p w_p(\theta_p - \overline{\theta})\right) - z\left(-K_\phi\partial_z\overline{b} + a_p w_p(b_p - \overline{b})\right)\right) \tag{70}$$

and the conservative temperature equation is

$$\partial_t\overline{\theta} = \frac{\overline{\epsilon}_\nu}{c_p - \alpha g z} - \partial_z\left(-K_\phi\partial_z\overline{\theta} + a_p w_p(\theta_p - \overline{\theta})\right)$$

A summary of EDMF energy budgets is provided in Fig. 1 and in Tab. 2.

4.6 Vertically integrated energy budgets

In this section, we provide global energy budgets to highlight the role of mass-flux terms in bulk energy exchange as well as sinks/sources at boundaries. Let us introduce the vertical average $\langle X\rangle_z = 1/(\sigma_o^a H)\int_0^{\sigma_o^a H} X\,\mathrm{d}z$, and the boundary operator $[X]_0^{\sigma_o^a H} = 1/(\sigma_o^a H)(X(z=\sigma_o^a H) - X(z=0))$. Then for any advected field X with source term S_X, we have (see Appendix D for a detailed derivation):

$$\begin{aligned} \frac{1}{2}\partial_t\left\langle\overline{X}^2\right\rangle_z = {} & \overbrace{-\left\langle K_X(\partial_z\overline{X})^2\right\rangle_z}^{<0} \quad \overbrace{-\left\langle\frac{E+D}{2}(X_p - \overline{X})^2\right\rangle_z}^{<0} \\ & + \left\langle\overline{X}\,\overline{S}_X\right\rangle_z + \left\langle a_p(S_X)_p(X_p - \overline{X})\right\rangle_z \\ & - \left[\overline{X}\,\overline{w'X'} + a_p w_p\frac{(X_p - \overline{X})^2}{2}\right]_0^{\sigma_o^a H} \end{aligned}$$

Consequently, the entrainment and detrainment processes contribute on average to decreasing the mean variance, similar to eddy-diffusivity terms. Although not sufficient in the context of nonlinear equations, monotonically decreasing variance is usually a necessary property to ensure analytical well-posedness of transport partial differential equations (e.g. Evans, 2010). Interestingly, the last term of the budget implies that a non-zero MF flux at the boundary leads to an additional sink of resolved variance (which is exactly compensated by an equal and opposite boundary source for $\overline{X'^2}$).

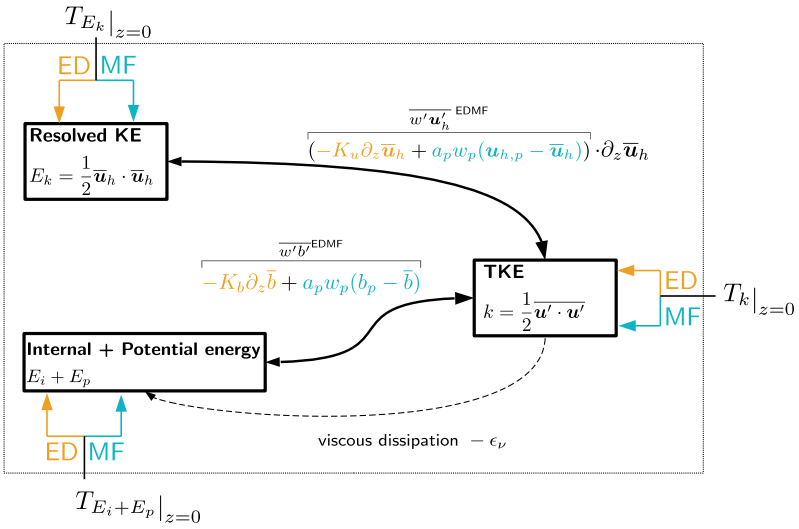

Figure 1: Schematic representation of bulk and boundary energy fluxes within EDMF closure (KE: kinetic energy, TKE: turbulent kinetic energy).

We use (71) to get the vertically integrated mean kinetic energy budget,

$$\begin{aligned}\partial_t \langle E_k \rangle_z &= -\left\langle K_u (\partial_z \overline{\boldsymbol{u}}_h)^2 \right\rangle_z - \left\langle \frac{E+D}{2(1-C_u)} (\boldsymbol{u}_{h,p} - \overline{\boldsymbol{u}}_h)^2 \right\rangle_z \\ &\quad - \left[\overline{\boldsymbol{u}}_h \cdot \overline{w'\boldsymbol{u}'_h} \right]_0^{\sigma_o^a H} - \left[\frac{a_p w_p}{2(1-C_u)} (\boldsymbol{u}_{h,p} - \overline{\boldsymbol{u}}_h)^2 \right]_0^{\sigma_o^a H}\end{aligned}$$

and the vertically integrated TKE budget

$$\begin{aligned}\partial_t \langle k \rangle_z &= -\left\langle K_\phi \partial_z \overline{b} \right\rangle_z + \left\langle a_p w_p (b_p - \overline{b}) \right\rangle_z \\ &\quad + \left\langle K_u (\partial_z \overline{\boldsymbol{u}}_h)^2 \right\rangle_z + \left\langle \frac{E+D}{2(1-C_u)} (\boldsymbol{u}_{h,p} - \overline{\boldsymbol{u}}_h)^2 \right\rangle_z \\ &\quad - \langle \overline{\epsilon}_\nu \rangle_z - [T_k]_0^{\sigma_o^a H} + \left[\frac{a_p w_p}{2(1-C_u)} (\boldsymbol{u}_{h,p} - \overline{\boldsymbol{u}}_h)^2 \right]_0^{\sigma_o^a H}\end{aligned}$$

It is interesting to note that the parameterization of the plume horizontal pressure gradient introduced in 2.3.2 and characterized by the parameter C_u induces a hyperbolic enhancement of the transfer from E_k to k due to entrainment/detrainment processes. Additionally, the vertically integrated potential energy and resolved internal energy budget reads

$$\partial_t \langle E_i + E_p \rangle_z = \left\langle K_\phi \partial_z \overline{b} \right\rangle_z - \left\langle a_p w_p (b_p - \overline{b}) \right\rangle_z + \langle \overline{\epsilon}_\nu \rangle_z - \left[T_{E_i+E_p} \right]_0^{\sigma_o^a HH} \tag{71}$$

To illustrate potential biases, let us examine the atmospheric surface flux at $z = 0$

$$T_{E_i+E_p}(0) = -c_p K_\theta \partial_z \overline{\theta}(0) + c_p a_p(0) w_p(0) (\theta_p(0) - \overline{\theta}(0))$$

and assume that the boundary condition is $-K_\theta \partial_z \overline{\theta}(0) = \overline{w'\theta'}(0)$ (for instance using MOST), along with a plume initialization of the form (28). Then we would have

$$T_{E_i+E_p}(0) = c_p \overline{w'\theta'}(0) + c_p \overline{w'\theta'}(0) \frac{a_p(0) w_p(0) \beta}{\sqrt{k(0)}}$$

$\partial_t E_k + \partial_z T_{E_k}$	$= -K_u(\partial_z \overline{\boldsymbol{u}}_h)^2 + a_p w_p(\boldsymbol{u}_{h,p} - \overline{\boldsymbol{u}}_h)\cdot\partial_z\overline{\boldsymbol{u}}_h$	Resolved kinetic energy budget
$\partial_t\left(E_i + E_p\right) + \partial_z T_{E_i+E_p}$	$= -\left(-K_\phi\partial_z\overline{b} + a_p w_p(b_p - \overline{b})\right) + \overline{\epsilon}_\nu$	Internal and potential energy budget
$\partial_t k - \partial_z\left(K_k\partial_z k\right)$	$= K_u(\partial_z\overline{\boldsymbol{u}}_h)^2 - K_\phi\partial_z\overline{b}$	ED related TKE production terms
	$-a_p w_p(\boldsymbol{u}_{h,p} - \overline{\boldsymbol{u}}_h)\cdot\partial_z\overline{\boldsymbol{u}}_h + a_p w_p(b_p - \overline{b})$	MF related TKE production terms
	$-\partial_z\left(a_p w_p\left[k_p - k + \frac{1}{2}\|\boldsymbol{u}_p - \boldsymbol{u}\|^2\right]\right)$	MF related TKE transport term
	$-\overline{\epsilon}_\nu$	TKE dissipation
$a_p w_p\partial_z k_p$	$= E\left(k - k_p + \frac{1}{2}\|\boldsymbol{u}_p - \boldsymbol{u}\|^2\right) - a_p(\epsilon_\nu)_p$	Plume related TKE
K_k	$= c_k l_m\sqrt{k}$	TKE eddy-diffusivity

Table 2: Complementary equations to those presented in Tab. 1, derived from energy consistency constraints in Sec. 4.

where the second term leads to an unphysical source of energy for $a_p(0)w_p(0) \neq 0$. This bias is due to an inconsistent partioning of the physical boundary flux $c_p\overline{w'\theta'}(0)$into ED and MF fluxes.

5 Evaluation of the EDMF-Energy scheme using a single column model

In this section, we numerically evaluate the proposed EDMF formulation on three cases of oceanic deep convection. The first two cases are performed in an idealized setting and compared to Large Eddy Simulation (LES) data, whereas the last case is initialized and forced with realistic data and compared to *in situ* measurements at the LION buoy in the Mediterranean Sea.

5.1 Description of idealized cases

The two idealized cases considered are reminiscent of typical deep convective conditions in the ocean (e.g. Marshall & Schott, 1999), where convection into a initially resting ocean of constant stratification $\Delta\theta = 1\,\mathrm{K}/1000\,\mathrm{m}$ (corresponding $N_0^2 = 1.962 \times 10^{-6}\,\mathrm{s}^{-2}$) is triggered by a surface cooling of $Q_0 = -500\,\mathrm{W\,m}^{-2}$ (corresponding to a surface buoyancy loss of $B_0 = -2.456 \times 10^{-7}\,\mathrm{m^2 s^{-3}}$). In both cases, salinity is kept uniform at $S = 32.6\,\mathrm{psu}$. The first case (FC500) consists of free convection, where no wind stress is applied. In the second idealized case (W005_C500) a uniform wind stress along the meridional direction, of magnitude $(u_*^a)^2 = 0.05\,\mathrm{m^2\,s^{-2}}$, is applied. A summary of the parameters for each case can be found in table 3. To characterize wind-shear effects, we introduce the Froude number (Haghshenas & Mellado, 2019)

$$Fr_* = \frac{u_*^o}{N_0 L_0} \tag{72}$$

where the length scale $L_0 = (B_0/N_0^3)^{1/2}$ can be interpreted as an Ozmidov scale $(\overline{\epsilon_\nu}/N^3)^{1/2}$ (Garcia & Mellado, 2014) which is a measure of the smallest eddy size affected by a background stratification N_0^2 in a turbulent field characterized by a viscous dissipation rate ϵ_ν. After $t_f = 72\,\mathrm{h}$ of simulation leading to a mixed layer depth h (defined as the depth at which the buoyancy flux is minimum) of several hundred meters, various non-dimensional numbers can be used to characterize the flow. Their values can be found in Tab. 4. The ratio of the mixed layer depth to the Obukhov length (Obukhov (1971) and Zheng et

Table 3: Idealized cases parameters

Case	Q_0 ($\mathrm{W\,m^{-2}}$)	$(u_*^a)^2$ ($\mathrm{m^2\,s^{-2}}$)	N_0^2 ($\mathrm{s^{-2}}$)	t_f (h)	Fr_*
FC500	-500	0	1.962×10^{-6}	72	0
W005_C500	-500	0.05	1.962×10^{-6}	72	0.56

Table 4: Idealized cases non-dimensional parameters after 72 h of simulation

Case	h/L_{Ob}	Ri_h	Ri_*
FC500	∞	∞	97
W05_C500	5.7	310	97

al. (2021) in the oceanic context) h/L_{Ob}, where

$$L_{Ob} = \frac{(u_*^o)^3}{-B_0}$$

is an estimate of the depth at which the production of TKE by turbulent shear is of the same order of magnitude as the production of TKE by buoyancy fluxes. Noting $w_* = (-B_0 h)^{1/3}$ the convective velocity scale (Deardorff, 1970), we get

$$\frac{h}{L_{Ob}} = \left(\frac{w_*}{u_*}\right)^3 \tag{73}$$

We also recall that the oceanic friction velocity u_*^o satisfies $\rho_o (u_*^o)^2 = \rho_a (u_*^a)^2$. The Richardson number at the mixed layer base,

$$Ri_h = \frac{N_0^2}{\left(\frac{u_*^o}{h}\right)^2}$$

measures the destabilization by surface shear stresses of a stably stratified water column. At $t_f = 72\,\mathrm{h}$, the case W005_C500 can be described by $h/L_{Ob} \simeq 5.7$ and $Ri_h \simeq 310$, which corresponds to a regime of strong deepening of the MLD according to Legay et al. (2023). Finally, for free convection cases (no wind) a convective Richardson number can be built as

$$Ri_* = \frac{N_0^2}{(w_*/h)^2} = \frac{N_0^2 h^{4/3}}{(-B_0)^{2/3}} = Ri_h \left(\frac{L_{Ob}}{h}\right)^{2/3}$$

It can be interpreted as follows. The time evolution of the mixed layer depth can be accurately described by the scaling (Turner, 1979; Van Roekel et al., 2018)

$$h \propto h_{\mathrm{enc}} \tag{74}$$

where the *encroachment* depth is $h_{\mathrm{enc}}(t) := \sqrt{2\frac{(-B_0)}{N_0^2}t}$. Then the ratio of the entrainment velocity $w_e = \frac{d}{dt}h$ to the convective velocity $w_* = (-B_0 h)^{1/3}$ reads

$$\frac{w_e}{w_*} \propto Ri_*^{-1} \tag{75}$$

5.2 LES model description and conditional sampling

The LES data have been generated by the Ocean-LES version of the non-hydrostatic model Méso-NH (Lac et al., 2018). It is solving an anelastic Lipps-Hemler system adapted

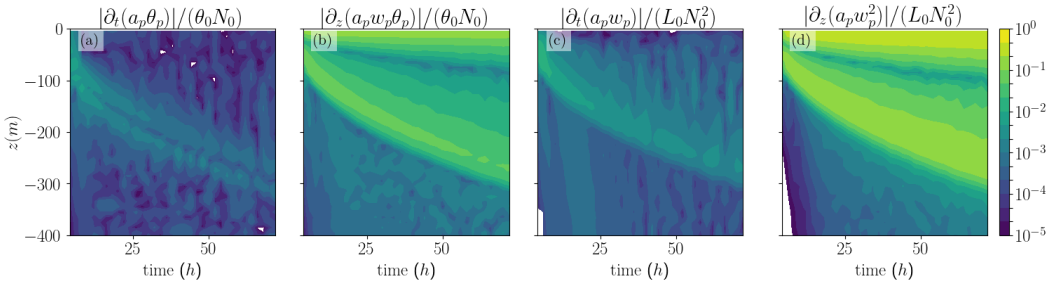

Figure 2: Temporal evolution of the normalized plume tendency $\partial_t(a_p X_p)$ and plume advection $\partial_z(a_p w_p X_p)$ terms, for the case FC500.

to the ocean, along with a linearized equation of state. The model uses a second-order Runge-Kutta time stepping and spatial discretization of advection operators is performed with a fourth-order centered scheme. Explicit subgrid scale closures are computed via a 3-D turbulence scheme based on a prognostic equation of the subgrid turbulent kinetic energy using a mixing-length scale, computed from the volume of a grid cell (Cuxart et al., 2000). The domain size is 1000 m on the vertical and 7.5 km×7.5 km on the horizontal, where doubly periodic conditions are applied. A resolution of 10 m on the vertical and 15 m on the horizontal is used. Each configuration is run for 72 h with a time-step of 10 s. To assess the quality of the simulations, we checked that the subgrid TKE was never exceeding 20% of the TKE explicitly resolved by the LES (Pope, 2004). Via analysis of the total TKE budget, we checked that a quasi-steady regime is reached after a few hours of simulation (e.g. Garcia & Mellado, 2014). Moreover, at the end of the simulations, the typical size of coherent structures, which can be quantified by the horizontal integral length scale in the bulk of the mixed layer, is of the order $O(500\,\mathrm{m}) \ll 7.5\,\mathrm{km}$. This suggests that the horizontal domain is large enough to provide a satisfactory sampling of turbulent structures.

To identify plumes, we use a velocity-based conditional sampling adapted from Pergaud et al. (2009), namely the plume area is defined as

$$A_p(z,t) = \left\{(x,y,z,t) \text{ such that } \overline{w}(z,t) - w(x,y,z,t) > m \times \max(\sqrt{\overline{w^{2\prime}}}(z,t), \sigma_{\min}(z,t))\right\} \quad (76)$$

where the minimum standard deviation is chosen as $\sigma_{\min}(z,t) = 0.05/(-z)\int_z^0 \sqrt{\overline{w^{2\prime}}}(z',t)\,\mathrm{d}z'$. We checked that the qualitative results were not sensitive to m, and used $m = 1$ for the remainder. We do not use the tracer-based sampling of Couvreux et al. (2010) since it is valid only for small variations of the mixed layer depth. We neither utilize the "strong updraft" sampling of (Siebesma et al., 2007) since it assumes that a_p is a given constant. However, we checked that similar conclusions could be drawn from such samplings (not shown).

5.3 Validity of the steady plume hypothesis and small area limit

In this section, we directly evaluate the validity of the assumptions made in Sec. 2.2 during the derivation of the proposed EDMF scheme against LES data. Fig. 2 shows that the plume temporal tendency terms are $O(10^{-2})$ smaller than plume advective terms which is consistent with the scaling in $1/(N_0 t)$ derived in 2.2.3. This justifies the use of the steady plume hypothesis. Fig. 3 shows vertical profiles of temperature, vertical velocity, plume fractional area, and temperature flux for the FC500 case. The small area assumption is roughly validated, with values of $a_p(z)$ between 10% and 20% of the total area, as exposed in previous studies (e.g. Couvreux et al., 2010). This justifies ques-

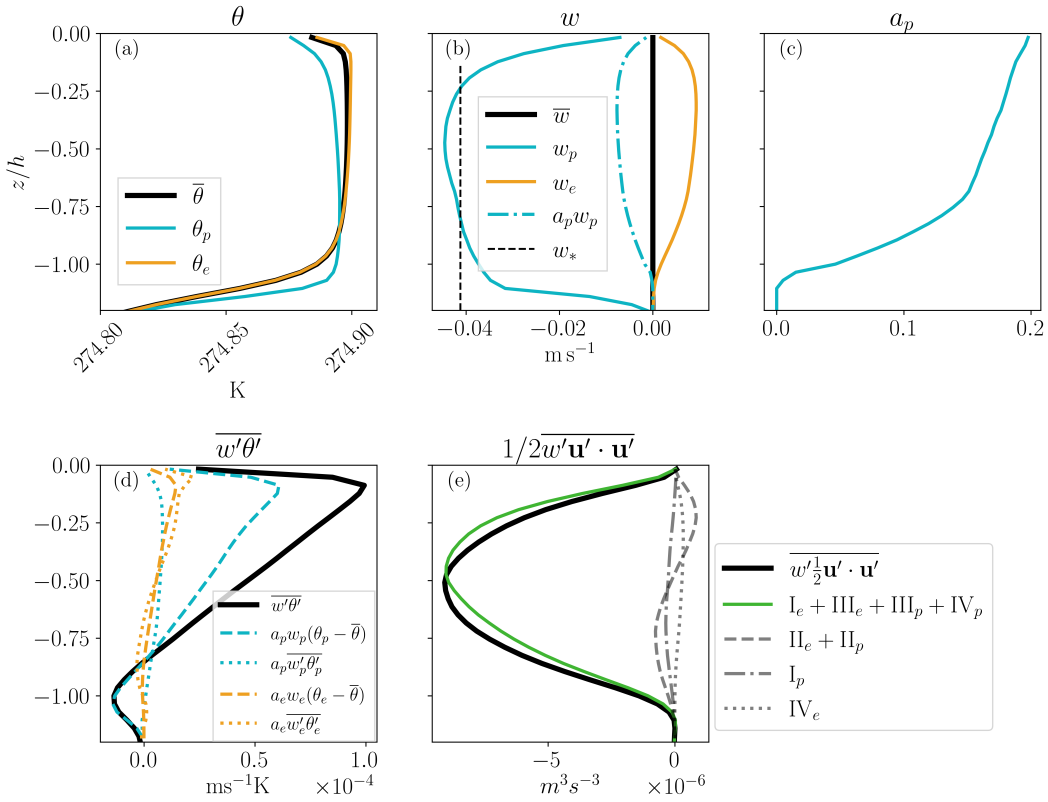

Figure 3: LES vertical profiles of (a) temperature, (b) vertical velocities, (c) plume fractional area, (d) temperature flux and (e) TKE flux for the FC500 case after 72 h of simulation. For each field, the black lines represent an horizontal average over the whole grid cell, the blue lines represent an average over the plume area and the orange lines represent an average over the environment area. In panel (b) the blue dotted line represents $a_p w_p$, and the gray dashed line represents the value of the free convective velocity scale w_*. In panel (d), total flux is in black, plume fluxes in blue (MF is dashed and subplume is dotted), and environment fluxes in orange (same linestyles). In panel (e) are represented the total flux (black) and the contributions from the combined terms $\mathrm{I}_e + \mathrm{III}_e + \mathrm{III}_p + \mathrm{IV}_p$ (blue), $\mathrm{II}_e + \mathrm{II}_p$ (dashed gray), I_p (dash-dotted gray) and III_p (dotted gray) (see 4.2 for details).

tioning the relevance of this assumption and considering the system described in Appendix A. The convective velocity w_* is found to be a good estimate of the plume vertical velocity w_p. The contribution of the mass-flux term $a_p w_p(\theta_p - \overline{\theta})$ to the total temperature flux is increasing with depth, until reaching a quasi-perfect match in the entrainment layer. The rough validity of assumption $a_p w_p(\theta_p - \overline{\theta}) \gg a_p\overline{w'_p\theta'_p}, a_e w_e(\theta_e - \overline{\theta})$ is consistent with the rough validity of $a_p \ll 1$. The plume/environment decomposition of the vertical transport of TKE $1/2\overline{w'\boldsymbol{u}'\cdot\boldsymbol{u}'}$ is presented in Fig. 3(e). The dominant terms exposed in (54) explain well the total flux.

All the previous findings are also verified for the W005_C500 case (not shown).

5.4 SCM evaluation

In this section, we evaluate three different configurations of the SCM against LES data. First, a setup where only an eddy-diffusivity closure is used (refered as "ED"), and

where the TKE equation (48) does not contain MF terms, which is equivalent to setting $a_p w_p = 0$. Second, an EDMF scheme in which an ED closure of the TKE equation (48) is used (referred as "EDMF"). This configuration is not energetically consistent as explained in Sec. 4. It would be the result of a naive independent coupling of TKE and MF schemes. Finally, the third configuration consists of the previously detailed EDMF scheme in which the TKE equation is modified as in (69) to include the contribution of MF terms to energy transfers (referred to as "EDMF-Energy"). Since the small area hypothesis is approximately valid in LES, we also tested the relaxed version of table 1. However, we could not identify significant impacts on such an idealized setup (not shown). For the three configurations, the constants c_m, c_ϵ, c_k used in the ED terms are the same as the constants used in the TKE equation of the LES model. The parameters used for the plume equations closures have been chosen as $\beta_1 = 0.99, \beta_2 = 1.99, a = 1.0, b = 1.25, b' = 0.003\,\mathrm{m}^{-1}, C_u = 0.5, a_p^0 = 0.2, \delta_0 = 0.005\,\mathrm{m}^{-1}$. A careful tuning and uncertainty quantification of the parameters, using for instance statistical method (e.g. Souza et al., 2020; Couvreux et al., 2021), is left for future studies.

The examination of mean temperature and flux of temperature profiles shows that ED fails to reproduce the so-called vertical entrainment zone (e.g. Garcia & Mellado, 2014), in which penetrative convection generates negative temperature flux and sharpens the temperature gradients at the base of the mixed layer. The lack of penetrative convection is known to reduce the deepening rate (e.g. chap. 6, Garratt, 1994a), thus producing an important bias of a hundred meters regarding the mixed layer depth compared to LES. On the other hand, EDMF and EDMF-energy equally perform in representing these profiles. The absence of a noticeable effect of the energetic consistency on the temperature mean and flux profiles is a consequence of the small value of the ED fluxes (dashed lines) in the mixed layer. When considering the TKE profile, ED can model the correct order of magnitude, however, the TKE does not penetrate enough. EDMF fails to reproduce TKE due to energetic inconsistency. Indeed, looking at temperature and velocity fluxes allows us to infer that the losses of resolved energy due to buoyancy and shear are dominated by the MF contributions. However, such contributions are not included as sources of TKE for the EDMF scheme, leading to the very low levels of TKE observed in the simulation. EDMF-energy can reproduce accurate profiles of TKE. The main discrepancies arise close to the surface and at the base of the mixed layer. Neither ED nor EDMF can reproduce the vertical transport of TKE, whereas EDMF-energy reproduces well the profile. Similar conclusions are drawn from the WC005_C500 case (see Fig. 5).

In Fig. 6, we represent the vertically integrated energy budget of the SCM for the case W005_C500 (FC500 is similar), namely the quantity

$$\int_{-H}^{0} \partial_t \left(E_k + k + E_i + E_p\right) \mathrm{d}z + \left[T_{E_k} + T_k + T_{E_i+E_p}\right]_{-H}^{0} \tag{77}$$

As expected, EDMF-energy conserves energy, whereas EDMF does not. The energy loss due to inconsistent energetics is equal to

$$\int_{-H}^{0} \left(-a_p w_p (b_p - \overline{b}) + a_p w_p (\boldsymbol{u}_{h,p} - \overline{\boldsymbol{u}}_h) \cdot \partial_z \overline{\boldsymbol{u}}_h\right) \mathrm{d}z \tag{78}$$

and scales with $B_0 h$.

5.5 Realistic case: Hymex/ASICS-MED campaign

We now move to more realistic situations corresponding to a sequence of strong convective events which were documented in the Northwestern Mediterranean during the winter 2013 of the HyMeX/ASICS-MED experiment at the LION buoy. This experiment was also carried out by Giordani et al. (2020) and we use a similar setup here (similar vertical grid as well as similar initial and surface boundary conditions). The experiments

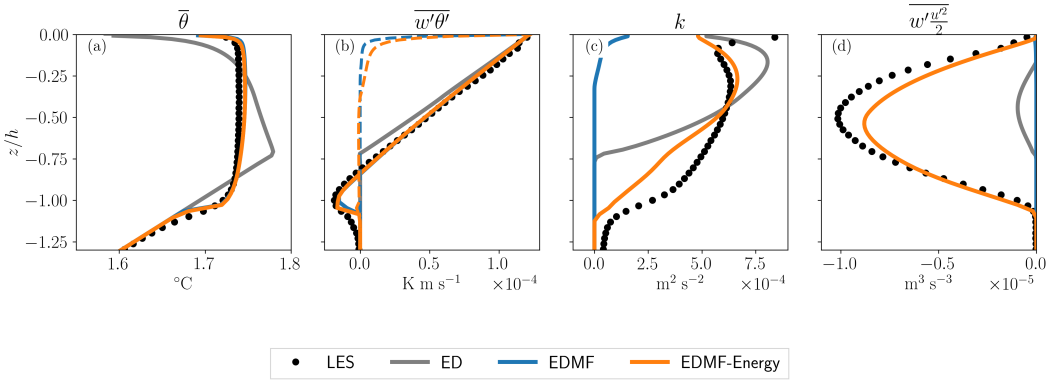

Figure 4: Vertical profiles of (a) temperature, (b) temperature flux, (c) turbulent kinetic energy and (d) turbulent transport of TKE for the FC500 case after $72h$ of simulation. LES data (black dots), ED-only scheme (grey line), standard EDMF scheme (blue line) and energetically consistent EDMF (orange line) are represented, along with the ED contribution to the temperature fluxes (dashed lines).

are performed with a SCM similar to (6) and (7) but including additional Coriolis and solar penetration (using a standard Jerlov law) terms. We consider conservative temperature and salinity as entropic variables which are related to buoyancy via a nonlinear equation of state. We also include penalization terms in the SCM to account for the effect of the bottom (which is at a depth of 2400 m at the LION buoy). Thanks to the penalization term a no-slip boundary condition is imposed at the bottom and a no-gradient condition is imposed for tracers. The vertical grid resolution ranges from 1 m near the surface to 150 m near the bottom located at $z = -2400$ m. Parameters of the TKE scheme are set to the standard NEMO values, $\boldsymbol{c} = (c_m, c_\epsilon, c_k) = (0.1, \frac{\sqrt{2}}{2}, 0.1)$.

A series of 30-days numerical simulations were carried out starting from January 15, 2013. The surface boundary conditions are shown in Fig. 7. In particular, very strong cooling events occurred during the period of interest. Two simulations were made systematically with an eddy-diffusivity term activated. A first simulation was done with Enhanced Vertical Diffusion (referred to as ED+EVD) which is the standard practice for climate simulations using NEMO, a second one using a mass flux scheme on tracers, dynamics, and with the additional terms for energetic consistency in the TKE equation (referred to as EDMF-energy). To get a more concrete idea of the improvements brought about by the mass flux scheme over the usual practice for NEMO applications (ED+EVD), we show in Fig. 7 (bottom panel) the temporal evolution of the mixed layer depth h_{mxl} computed from mooring data and single-column numerical simulations. h_{mxl} is defined as the depth where the following criterion is met

$$\int_{h_{\mathrm{mxl}}}^{z_{\mathrm{ref}}} \partial_z b_{\mathrm{eos}}(\theta, S = 38.5 \text{ psu})\, dz = \frac{g}{\rho_0}\rho_c$$

with $z_{\mathrm{ref}} = 300$ m and $\rho_c = 0.01$ kg m^{-3}. We had to consider a constant salinity in the buoyancy calculation because the salinity data from the LION buoy are noisy in the vertical and did not allow for a robust diagnostics.The bottom panel in Fig. 7 illustrates the fact that the penetration depth of convective plumes is significantly better represented by the EDMF-Energy scheme than by the ED+EVD approach. Moreover, a direct comparison with temperature and salinity from mooring data is shown in Fig. 8 at different times. In particular several phases can be identified during the experiment (e.g. Coppola et al., 2017; Waldman et al., 2017): (*i*) in the period 15-25 January 2013 winter convection starts to deepen the mixed layer down to around −800 m to the point of erod-

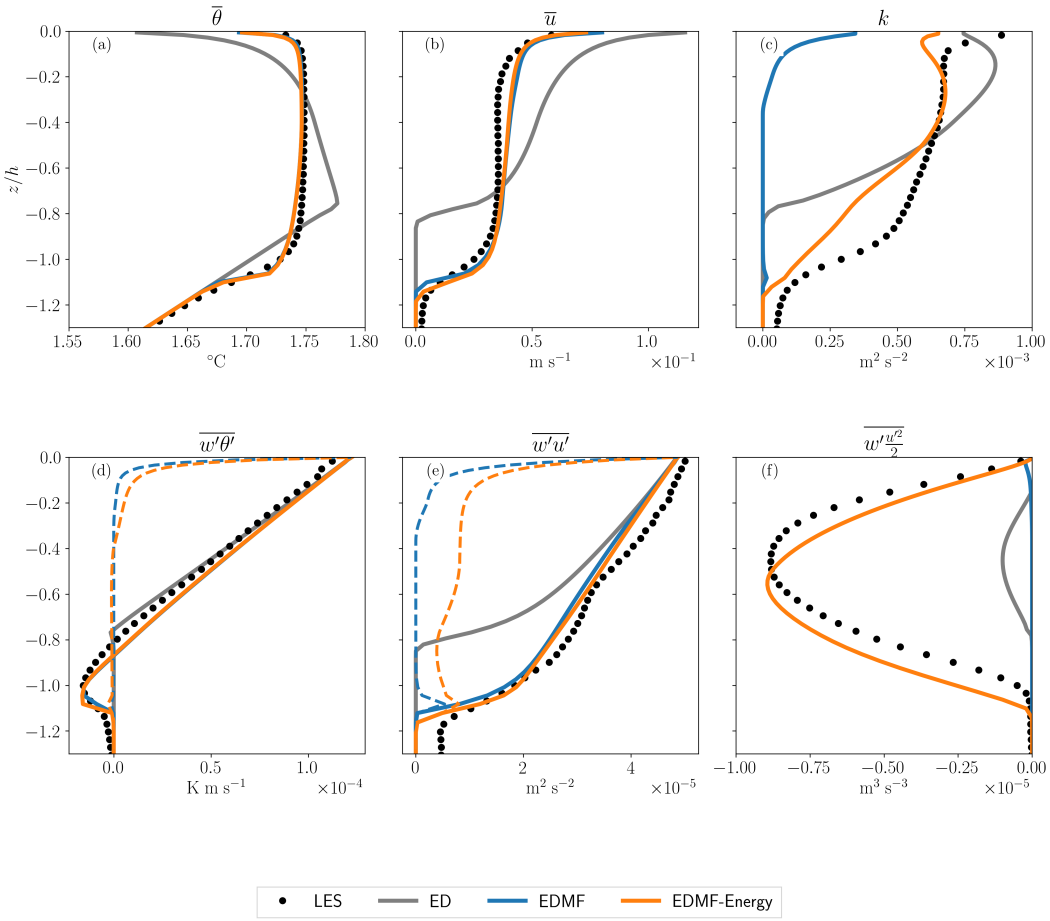

Figure 5: Vertical profiles of (a) mean temperature, (b) mean zonal current, (c) turbulent kinetic energy, (d) temperature flux, (e) zonal momentum flux, (d) turbulent transport of TKE for the FC500 case after $72h$ of simulation. LES data (black dots), ED-only scheme (grey line), standard EDMF scheme (blue line) and energetically-consistent EDMF (orange line) are represented, along with the ED contribution to the temperature and momentum fluxes (dashed lines).

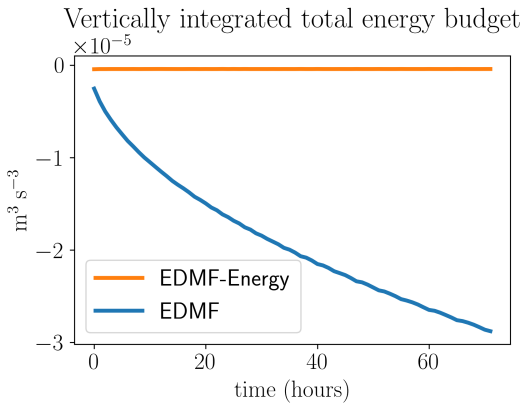

Figure 6: Time series of the vertically integrated energy budget (77) for the case W005_C500 (see text for details).

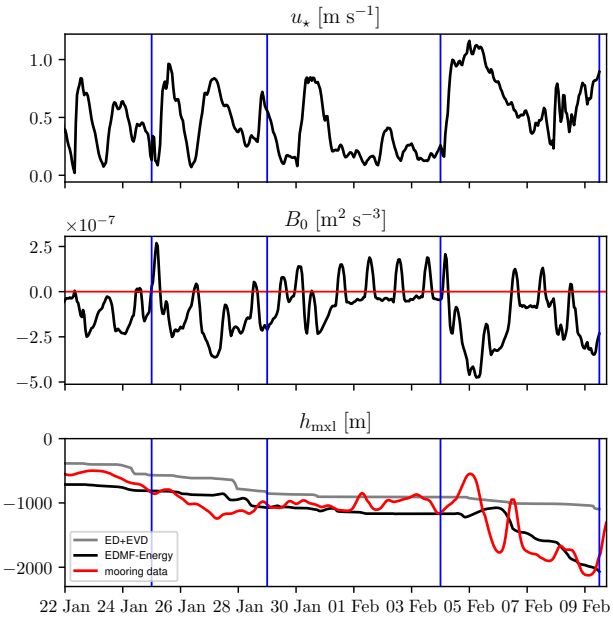

Figure 7: Time series of the friction velocity $u_\star$ (m s^{-1}, top panel) and surface buoyancy flux B_0 (m^2 s^{-3}, middle panel) computed from atmospheric forcings. Time series of mixed layer depth h_{mxl} (m, bottom panel) obtained from observations at the LION buoy (red line) and from single column numerical experiments using ED+EVD (solid gray line) and EDMF-Energy (solid black line). The vertical blue lines correspond to the dates at which the vertical temperature and salinity profiles derived from observations and numerical simulations are compared in Fig. 8.

ing the Levantine intermediate waters. (*ii*) in the period 26–29 January 2013 the mixed layer keeps thickening to the depth of the western Mediterranean deep water (≈ -1250 m) (*iii*) in the period 4-9 February 2013 a new intense convective event associated with a strong Mistral event contributes to deepen the mixed layer down to the bottom (reached in 9 February). This is followed by a restratification phase involving horizontal processes that cannot be represented in our SCM formalism which explains why we do not analyze solutions beyond February 9.

6 Discussion and conclusion

In this work, we have presented the theoretical derivation of an EDMF scheme with special attention paid to energetic aspects in a simple thermodynamic setting, for both dry atmosphere and seawater with linearized equation of state. During the derivation, we systematically reviewed the approximations used and provided both *a priori* scaling estimations, and direct evaluations of their validity on two idealized LES of oceanic convection. Closed energetics at the SCM level is a necessary step to obtain energetically consistent 3D models and thus reduce spurious energy biases. Theoretical horizontally averaged energy budgets are guiding the derivation of consistent energy budgets for SCM with EDMF closure. In particular, we have exposed the necessary modification of the standard TKE equation that incorporates EDMF terms to obtain closed energy budgets. Besides taking into account MF terms in shear and buoyancy terms, we propose an MF parameterization of TKE transport based on LES diagnostics. It generalizes previous formulations and implies the consideration of a subplume TKE (Han & Bretherton, 2019).

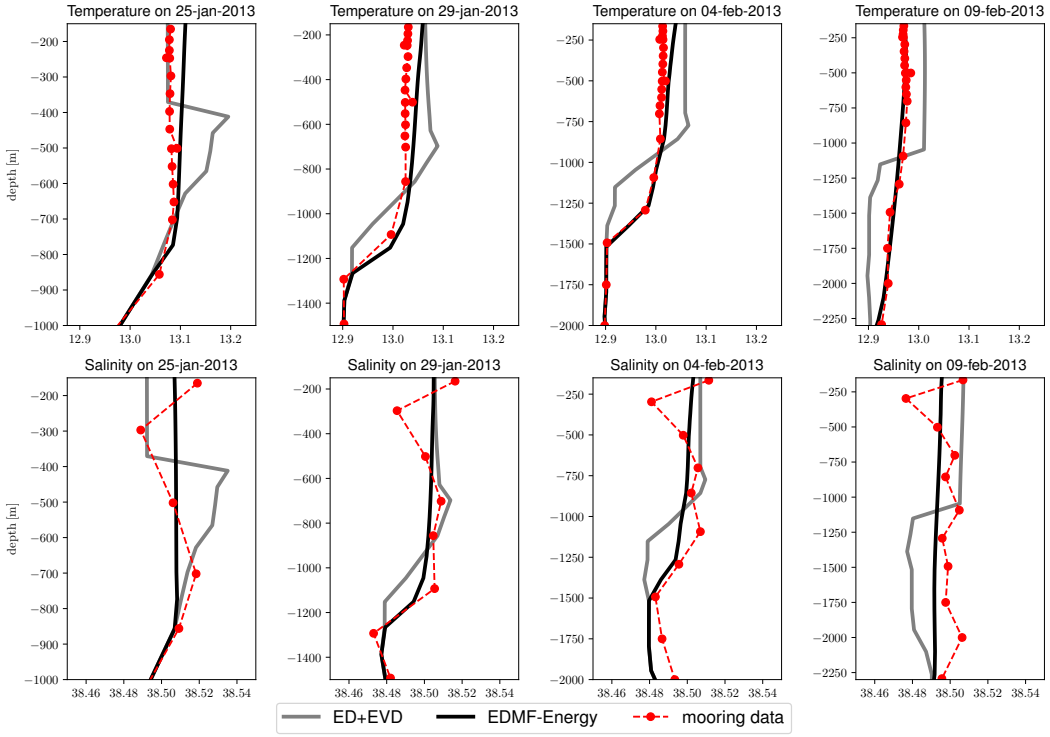

Figure 8: Temperature (^{o}C, top panels) and salinity (psu, bottom panels) profiles obtained from single column experiments at the location of the LION buoy using an eddy-diffusivity closure with enhanced vertical diffusion (ED-EVD, solid gray lines) and energetically-consistent EDMF (EDMF-Energy, solid black lines). Results from numerical experiments are compared to observations from the LION buoy (dashed red lines) for 4 dates represented on the Fig. 7 by vertical blue lines.

We also show that boundary conditions on both mean and plume variables should be consistent with the EDMF decomposition to avoid spurious energy fluxes at the boundary and subsequent inconsistent energetics. We evaluate the performance of the proposed energetically consistent EDMF scheme in the context of idealized oceanic convection. When compared with LES of idealized oceanic convection, our scheme can reproduce mean fields and vertical fluxes of temperature and momentum as well as a non-energetically closed EDMF scheme. However energetic consistency is key to obtaining realistic TKE and turbulent transport of TKE profiles. To further illustrate that the MF concept is a credible alternative to the traditional approaches used in the oceanic context (using an enhanced vertical diffusion or a counter gradient term *à la* KPP (Large et al., 1994)) the proposed scheme is validated in a single-column configuration against observational data of oceanic convection from the LION buoy.

Even if the proposed derivation may seem tedious, the energetically consistent parameterization obtained is rather simple to implement, whether in a code with an existing "non-energetically consistent" EDMF scheme or, more generally, in any code relying on a prognostic TKE equation. The MF terms are obtained by solving a straightforward system of ODEs and take the form of vertical advection terms in the mean equations (see Appendix F for practical details). The proposed approach can also be applied in the case where the ED closure does not use TKE. In this case, it would require to add a prognostic or diagnostic TKE equation (even if it does not interact with the ED term) to enforce energetic consistency.

This paper was intentionally oriented toward the theoretical description of energetically consistent EDMF schemes. The first idealized test cases were not conclusive on several new aspects which should be further assessed using more realistic SCM/LES intercomparisons in future studies. Among these aspects, we can mention: the impact of choosing the total TKE k instead of the environmental TKE k_e to compute eddy-diffusivities (sec. 2.3.3); the impact of relaxing the small-area assumption presented in Appendix A; the impact of energetic consistency on the accuracy of the mean fields.

The development of energetically consistent EDMF schemes can be continued in several ways. First, for real-world applications, the present work has to be extended to more complex thermodynamics models (i.e. moist atmosphere, Pauluis (2008), and seawater with a non-linear equation of state, Tailleux and Dubos (2023)). As a starting point, we provided in Appendix E a derivation of EDMF energy budgets in the anelastic setting from a dry atmosphere. The proposed framework is flexible enough to be readily extended to other coherent structures of the boundary layer contributing to transport, such as atmospheric downdraft (Han & Bretherton, 2019; Brient et al., 2023). For atmospheric models, the ED-based Monin-Obukhov similarity theory should be reconciled with the EDMF representation of fluxes (Li et al., 2021) to provide unambiguous and consistent boundary conditions and thus avoid potential spurious boundary energy fluxes.

To implement and then assess the impact of this energetically consistent parameterization on realistic 3D oceanic simulations a calibration of the remaining "free" parameters must be achieved (Hourdin et al., 2017; Couvreux et al., 2021). It should be performed on parameters whose universality can sometimes be statistically assessed (Souza et al., 2020), and should be mathematically and physically constrained as much as possible (see e.g. section 4.6). We believe that designing energetically consistent parameterization is a way to achieve more realistic models before their tuning.

Appendix A Relaxing the small area limit

The small-area assumption can be relaxed with no additional complexity if the subplume fluxes $\overline{w_p' \phi_p'}$ are still neglected. A summary of the EDMF-Energy parameterization in such a regime is presented in Tab. A1.

$\widetilde{\alpha}$	$= \dfrac{1}{1-a_p}$	Rescaling coefficient
$\overline{w'\phi'}$	$= \widetilde{\alpha} a_p w_p (\phi_p - \overline{\phi}) - K_\phi \partial_z \overline{\phi}$	Vertical turbulent flux for component ϕ
$\overline{w'\boldsymbol{u}'_h}$	$= \widetilde{\alpha} a_p w_p (\boldsymbol{u}_{h,p} - \overline{\boldsymbol{u}}_h) - K_m \partial_z \overline{\boldsymbol{u}}_h$	Vertical turbulent momentum flux
$\partial_z(a_p w_p)$	$= E - D$	Plume area conservation equation
$a_p w_p \partial_z \phi_p$	$= \widetilde{\alpha} E (\overline{\phi} - \phi_p)$	Plume equation for component ϕ
$a_p w_p \partial_z \boldsymbol{u}_{h,p}$	$= \widetilde{\alpha} E (\overline{\boldsymbol{u}}_h - \boldsymbol{u}_{h,p}) + a_p w_p C_u \partial_z \overline{\boldsymbol{u}}_h$	Plume horizontal momentum equation
$a_p w_p \partial_z w_p$	$= -(\widetilde{\alpha} b) E w_p + a_p \left\{ a B_p - \sigma_o^a (\widetilde{\alpha} b') w_p^2 \right\}$	Plume vertical velocity equation
B_p	$= b_{\text{eos}}(\phi_p) - b_{\text{eos}}(\overline{\phi})$	Buoyancy forcing term
$\partial_t k - \partial_z \left(K_k \partial_z k \right)$	$= K_m (\partial_z \overline{\boldsymbol{u}}_h)^2 - K_\phi \partial_z \bar{b}$	ED related TKE production terms
	$-\widetilde{\alpha} a_p w_p \left((\boldsymbol{u}_{h,p} - \overline{\boldsymbol{u}}_h) \cdot \partial_z \overline{\boldsymbol{u}}_h - (b_p - \bar{b}) \right)$	MF related TKE production terms
	$-\partial_z \left(\widetilde{\alpha} a_p w_p \left[k_p - k + \dfrac{1}{2} \lVert \boldsymbol{u}_p - \boldsymbol{u} \rVert^2 \right] \right)$	MF related TKE transport term
	$-\bar{\epsilon}_\nu$	TKE dissipation
$a_p w_p \partial_z k_p$	$= \widetilde{\alpha} E \left((k - k_p) + \dfrac{1}{2} \lVert \boldsymbol{u}_p - \boldsymbol{u} \rVert^2 \right) - a_p (\epsilon_\nu)_p$	Plume related TKE

Table A1: Same as table 1, but with a relaxation of the small area limit. Note that under the small area limit we would have $\widetilde{\alpha} \equiv 1$.

Appendix B Mixing length computations

For the oceanic applications detailed in this article, we have chosen a formulation of eddy-diffusivity and viscosity close to that used in the NEMO ocean model (Madec et al., 2019). The eddy-viscosity and diffusivity are classically assumed to be related to TKE by

$$\begin{aligned} K_u &= c_m l_m \sqrt{k} \\ K_\phi &= K_u (\text{Pr}_t)^{-1} \end{aligned}$$

with l_m a mixing length scale, Pr_t the non-dimensional turbulent Prandtl number, and c_m is a constant ($c_m = 0.1$ in NEMO). The mixing length l_m is calculated in two steps by considering separately the length scales l_{up} and l_{dwn} associated respectively to upward and downward movements : (1) l_{up} and l_{dwn} are initialized assuming $l_{\text{up}} = l_{\text{dwn}} = \sqrt{2k}\tau_{\text{ed}}$ with τ_{ed} a characteristic time equal to $1/N = (\partial_z \bar{b})^{-1}$ (2) a physical limitation is used to guarantee that l_{up} and l_{dwn} do not exceed the distance to the top and the bottom, this limitation amounts to controlling the vertical gradients of l_{up} and l_{dwn} such that they are not larger that the variations of depth (*e.g.* Madec et al., 2019). Once l_{up} and l_{dwn} are computed the mixing length is taken as $l_m = \min(l_{\text{up}}, l_{\text{dwn}})$. The turbulent Prandtl number is modelled by $\text{Pr}_t = \min(\text{Pr}_t^{\max}, \max(\text{Ri}/\text{Ri}_c, 1))$ with $\text{Ri} = N^2 / \lVert \partial_z \overline{\mathbf{u}}_h \rVert^2$, $\text{Pr}_t^{\max} = 10$ and $\text{Ri}_c = 0.2$.

Appendix C Boundary condition for plume equations

Near the surface, we linearize the plume and mean buoyancy in the form $b \simeq b^0 + b' z$. Then the plume equation for b_p reads at order $O(z^0)$:

$$a_p^0 w_p^0 b'_p = -E_0 (b_p^0 - \bar{b}^0)$$

The boundary condition $b_p^0 = \overline{b}^0$ implies that $b'_p = 0$. Thus we get

$$b_p(z) \simeq \overline{b}^0, \qquad \overline{b} \simeq \overline{b}^0 + N_0^2 z$$

Then near the surface, the buoyancy force - which is a source of plume momentum and kinetic energy $1/2w_p^2$ - is at first order $b_p - \overline{b} \simeq -N_0^2 z$. Consequently, any static instability at the surface will result in the absolute growth of the plume vertical momentum ($-N_0^2 z > 0$ in the atmosphere and $-N_0^2 z < 0$ in the ocean).
The boundary condition $b_p(0) = \overline{b}(0)$ implies that at $z = 0$, all the surface flux is allocated in the ED component. Consequently, $N_0^2 = \overline{w'b'}(0)/(-K_b(0)) = \overline{w'b'}(0)/(c_b l_b(0)\sqrt{k(0)})$.
The boundary condition $b_p(0) = \overline{b}(0)$ thus implies that close to the surface

$$b_p(z) \simeq \overline{b}(z) + \frac{\overline{w'b'}(0)}{c_b l_b(0)\sqrt{k_0}} z$$

Appendix D EDMF Mean Variance Equation

Start from the mean and plume equations, and the turbulent flux decomposition

$$\begin{aligned}
\partial_t \overline{X} &= -\partial_z \overline{w'X'} + \overline{S}_X && \text{(D1)}\\
\overline{w'X'} &= -K_X \partial_z \overline{X} + a_p w_p (X_p - \overline{X}) && \text{(D2)}\\
a_p w_p \partial_z X_p &= -E(X_p - \overline{X}) + a_p S_{X,p} && \text{(D3)}
\end{aligned}$$

Multiplying the mean equation (D1) by $\overline{X}$ leads to

$$\begin{aligned}
\frac{1}{2}\partial_t \overline{X}^2 &= -\partial_z(\overline{X}\,\overline{w'X'}) + \overline{w'X'}\partial_z\overline{X} + \overline{X}\,\overline{S_X}\\
&= -\partial_z(\overline{X}\,\overline{w'X'}) - K_X(\partial_z\overline{X})^2 + a_p w_p (X_p - \overline{X})\partial_z\overline{X} + \overline{X}\,\overline{S_X} && \text{(D4)}
\end{aligned}$$

To rewrite the second term of the right-hand side, we use the plume equation (D2):

$$\begin{aligned}
a_p w_p (X_p - \overline{X})\partial_z \overbrace{\overline{X}}^{=X_p+(\overline{X}-X_p)} &= -E(X_p - \overline{X})^2 + (X_p - \overline{X}) a_p S_{X,p}\\
&\quad -a_p w_p \frac{1}{2}\partial_z (X_p - \overline{X})^2\\
&= -E(X_p - \overline{X})^2 + (X_p - \overline{X}) a_p S_{X,p}\\
&\quad -\partial_z\left(a_p w_p \frac{1}{2}(X_p - \overline{X})^2\right)\\
&\quad +(E - D)\frac{1}{2}(X_p - \overline{X})^2\\
&= -(E + D)\frac{1}{2}(X_p - \overline{X})^2 + (X_p - \overline{X}) a_p S_{X,p}\\
&\quad -\partial_z\left(a_p w_p \frac{1}{2}(X_p - \overline{X})^2\right)
\end{aligned}$$

Using this expression into equation (D4), then vertically integrating the variance budget leads to the desired equation (71).

Appendix E Anelastic energy budgets

In this appendix, we derive energy budgets for a general anelastic model commonly used in atmospheric models. We start with the unaveraged anelastic mass and momentum budgets:

$$\begin{aligned}
\nabla \cdot (\rho_{\text{ref}} \boldsymbol{u}) &= 0 && \text{(E1)}\\
\partial_t \boldsymbol{u} &= -\nabla \cdot (\boldsymbol{u} \otimes \boldsymbol{u}) - \boldsymbol{f} \times \boldsymbol{u} - \nabla\left(\frac{p^\dagger}{\rho_{\text{ref}}}\right) + b\boldsymbol{e}_z + \nu \nabla^2 \boldsymbol{u} && \text{(E2)}
\end{aligned}$$

where $\rho_{\text{ref}} = \rho_{\text{ref}}(z)$ is a reference density profile, and the total pressure is $p(x,y,z,t) = p_{\text{ref}}(z) + p^\dagger(x,y,z,t)$ where by definition $\partial_z p_{\text{ref}}(z) = -\rho_{\text{ref}} g$.

As in section 3, we keep the same notations for the specific mean kinetic energy $E_k = (\overline{\boldsymbol{u}}_h \cdot \overline{\boldsymbol{u}}_h)/2$, the turbulent kinetic energy $k = (\overline{\boldsymbol{u}' \cdot \boldsymbol{u}'})/2$, the potential energy $E_p = gz$ and the mean internal energy E_i. Note however that these *specific energies* have to be multiplied by ρ_{ref} to get corresponding energies.

E1 Kinetic energies

By using the SCM assumptions exposed in Sec. 2.1, we can derive budgets for the resolved kinetic energy E_k and the turbulent kinetic energy k:

$$\partial_t E_k + \frac{1}{\rho_{\text{ref}}}\partial_z T_{E_k} = \overline{w'\boldsymbol{u}'_h} \cdot \partial_z \overline{\boldsymbol{u}}_h \tag{E3}$$

$$\partial_t k + \frac{1}{\rho_{\text{ref}}}\partial_z T_k = -\overline{w'\boldsymbol{u}'_h} \cdot \partial_z \overline{\boldsymbol{u}}_h + \overline{w'b'} - \overline{\epsilon}_\nu \tag{E4}$$

where $\overline{\epsilon_\nu} = \nu\overline{\partial_z \boldsymbol{u}' \cdot \partial_z \boldsymbol{u}'}$ is the viscous dissipation of energy, $T_{E_k} = \rho_{\text{ref}}\overline{w'\boldsymbol{u}'_h} \cdot \overline{\boldsymbol{u}}_h$ and $T_k = \rho_{\text{ref}}\overline{w'\frac{\boldsymbol{u}'\cdot\boldsymbol{u}'}{2}} + \overline{w'p^{\dagger\prime}}$. Exchanges between the resolved and subgrid reservoirs of kinetic energy are done via the mechanical shear term $\overline{w'\boldsymbol{u}'_h}\cdot\partial_z\overline{\boldsymbol{u}}_h$. To close the budgets, we will provide in the following sections a budget of internal and potential energy.

E2 Internal and Potential energies

For a generic fluid, the unaveraged specific internal energy can be written as

$$\mathcal{E}_i = \hbar(p,\phi) - \frac{p}{\rho} \tag{E5}$$

where $\hbar$ is the specific enthalpy and ϕ is any entropic variable describing each component of the fluid. Within the context of anelastic approximation, internal energy becomes

$$\mathcal{E}_i = \hbar(p_{\text{ref}},\phi) - \frac{p_{\text{ref}}}{\rho_{\text{ref}}} \tag{E6}$$

In particular, it implies within the anelastic approximation that $b(\phi) := -g(\rho(p_{\text{ref}},\phi) - \rho_{\text{ref}})/\rho(p_{\text{ref}},\phi)$, where the specific volume can be defined as $1/\rho(p_{\text{ref}},\phi) = \partial_p\hbar(p_{\text{ref}},\phi)$. The unaveraged budget of internal and potential energy then reads

$$\partial_t(\mathcal{E}_i + E_p) + \frac{1}{\rho_{\text{ref}}}\nabla\cdot[\rho_{\text{ref}}(\hbar(p_{\text{ref}},\phi) + gz)\boldsymbol{u}] = \epsilon_\nu - wb \tag{E7}$$

Upon averaging and using the SCM assumptions, the budget of mean internal energy $E_i = \overline{\mathcal{E}}_i$ and potential energy reads

$$\partial_t(E_i + E_p) + \frac{1}{\rho_{\text{ref}}}\partial_z(\rho_{\text{ref}}\overline{\partial_\phi \hbar_{\text{ref}}}\,\overline{w'\phi'}) = \overline{\epsilon}_\nu - \frac{1}{\rho_{\text{ref}}}\partial_z(\rho_{\text{ref}}(\overline{\phi}\,\overline{w'\partial_\phi\hbar'_{\text{ref}}} + \overline{\phi' w'\partial_\phi \hbar'_{\text{ref}}})) - \overline{w'b'} \tag{E8}$$

where we introduced the notation $\hbar_{\text{ref}}(\phi) = \hbar(p_{\text{ref}},\phi)$. Remark that if $\hbar(p_{\text{ref}},\phi)$ is linear in ϕ, we have closed relations $\overline{\hbar(p_{\text{ref}},\phi)} = \hbar(p_{\text{ref}},\overline{\phi})$ and $\overline{b(\phi)} = b(\overline{\phi})$.

As a summary, the budgets of mean kinetic energy, turbulent kinetic energy and the sum of mean internal and potential energy are

$$\begin{cases} \partial_t E_k + \partial_z T_{E_k} & = \overline{w'\boldsymbol{u}'_h}\cdot\partial_z\overline{\boldsymbol{u}}_h \\ \partial_t k + \partial_z T_k & = -\overline{w'\boldsymbol{u}'_h}\cdot\partial_z\overline{\boldsymbol{u}}_h + \overline{w'b'} - \overline{\epsilon}_\nu \\ \partial_t(E_i+E_p) + \frac{1}{\rho_{\text{ref}}}\partial_z(\rho_{\text{ref}}\overline{\partial_\phi\hbar_{\text{ref}}}\,\overline{w'\phi'}) & = \overline{\epsilon}_\nu - \frac{1}{\rho_{\text{ref}}}\partial_z(\rho_{\text{ref}}\overline{\phi}\,\overline{w'\partial_\phi\hbar'_{\text{ref}}} + \overline{\phi' w'\partial_\phi\hbar'_{\text{ref}}}) - \overline{w'b'} \end{cases} \tag{E9}$$

where conversion of E_k into k occurs via mean shear, conversion of k into E_i occurs via viscous dissipation, and conversion of k into $E_i + E_p$ occurs via buoyancy fluxes.

For a *dry atmosphere* modeled as an ideal gas $p = \rho R_d T$, the specific enthalpy reads

$$\hbar(p_{\rm ref}, \theta) = c_p \left(\frac{p_{\rm ref}}{p_0}\right)^{R_d/c_p} \theta \tag{E10}$$

which is linear in the potential temperature $\theta = T\left(p/p_0\right)^{-R_d/c_p}$. and buoyancy is $b(\overline{\theta}) = g(\overline{\theta} - \theta_{\rm ref})/\theta_{\rm ref}$. The budget of $E_i + E_p$ is

$$\partial_t(E_i + E_p) = c_p \left(\frac{p_{\rm ref}}{p_0}\right)^{R_d/c_p} \partial_t \overline{\theta} = \overline{\epsilon}_\nu - \frac{1}{\rho_{\rm ref}} \partial_z \left(\rho_{\rm ref} c_p \left(\frac{p_{\rm ref}}{p_0}\right)^{R_d/c_p} \overline{w'\theta'}\right) - \frac{g}{\theta_{\rm ref}} \overline{w'\theta'} \tag{E11}$$

where $\theta_{\rm ref} = \left(\frac{p_{\rm ref}}{p_0}\right)^{-R_d/c_p} \frac{p_{\rm ref}}{\rho_{\rm ref} R_d}$. As a summary, the budgets of mean kinetic energy, turbulent kinetic energy and the sum of mean internal and potential energy for a *dry atmosphere* within the anelastic approximation are

$$\begin{cases} \partial_t E_k + \partial_z T_{E_k} & = \overline{w' \boldsymbol{u}_h'} \cdot \partial_z \overline{\boldsymbol{u}}_h \\ \partial_t k + \partial_z T_k & = -\overline{w' \boldsymbol{u}_h'} \cdot \partial_z \overline{\boldsymbol{u}}_h + \frac{g}{\theta_{\rm ref}} \overline{w'\theta'} - \overline{\epsilon}_\nu \\ c_p \left(\frac{p_{\rm ref}}{p_0}\right)^{R_d/c_p} \partial_t \overline{\theta} & = \overline{\epsilon}_\nu - \frac{1}{\rho_{\rm ref}} \partial_z \left(\rho_{\rm ref} c_p \left(\frac{p_{\rm ref}}{p_0}\right)^{R_d/c_p} \overline{w'\theta'}\right) - \frac{g}{\theta_{\rm ref}} \overline{w'\theta'} \end{cases} \tag{E12}$$

E3 EDMF-parameterized budget

Within the anelastic approximation, the budget of resolved kinetic energy, subgrid kinetic energy and resolved internal+potential energy for a *dry atmosphere* with EDMF closures is

$$\begin{cases} \partial_t E_k + \frac{1}{\rho_{\rm ref}} \partial_z T_{E_k} & = -K_u (\partial_z \overline{\boldsymbol{u}}_h)^2 + a_p w_p (\boldsymbol{u}_{\hbar,p} - \overline{\boldsymbol{u}}_h) \cdot \partial_z \overline{\boldsymbol{u}}_h \\ \partial_t k + \frac{1}{\rho_{\rm ref}} \partial_z T_k & = \frac{g}{\theta_{\rm ref}} \left[-K_\theta \partial_z \overline{\theta} + a_p w_p (\theta_p - \overline{\theta})\right] + K_u (\partial_z \overline{\boldsymbol{u}}_h)^2 - a_p w_p (\boldsymbol{u}_{\hbar,p} - \overline{\boldsymbol{u}}_h) \cdot \partial_z \overline{\boldsymbol{u}}_h - \overline{\epsilon}_\nu \\ \partial_t \left[c_p \left(\frac{p_{\rm ref}}{p_0}\right)^{R_d/c_p} \overline{\theta}\right] & = -\frac{1}{\rho_{\rm ref}} \partial_z T_{E_i+E_p} + \overline{\epsilon}_\nu - \frac{g}{\theta_{\rm ref}} \left[-K_\theta \partial_z \overline{\theta} + a_p w_p (\theta_p - \overline{\theta})\right] \end{cases} \tag{E13}$$

where the flux terms are

$$T_{E_k} = \rho_{\rm ref} \left(-K_u \partial_z \overline{\boldsymbol{u}}_h + a_p w_p (\boldsymbol{u}_{\hbar,p} - \overline{\boldsymbol{u}}_h)\right) \cdot \overline{\boldsymbol{u}}_h \tag{E14}$$

$$T_k = -\rho_{\rm ref} K_k \partial_z k + \rho_{\rm ref} a_p w_p \left(k_p - k + \frac{1}{2} \|\boldsymbol{u}_p - \overline{\boldsymbol{u}}\|^2\right) \tag{E15}$$

$$T_{E_i+E_p} = \rho_{\rm ref} c_p \left(\frac{p_{\rm ref}}{p_0}\right)^{R_d/c_p} \left(-K_\theta \partial_z \overline{\theta} + a_p w_p (\theta_p - \overline{\theta})\right) \tag{E16}$$

Appendix F Discretization of energetically consistent EDMF equations

We start from the standard grid arrangement used in oceanic models which are usually discretized on a Lorenz grid in the vertical (density is located in the center of the cells on the vertical). We consider N grid cells in the vertical with thickness $\Delta z_j = z_{j+1/2} - z_{j-1/2}$ ($z_{1/2} = -H$ and $z_{N+1/2} = 0$ the surface) such that $\sum_{j=1}^N \Delta z_j = -H$. Traditionally, the turbulent quantities like turbulent kinetic energy k and eddy diffusivities K_X are naturally located on the interfaces at $z_{j+1/2}$ to avoid interpolations when computing the vertical gradients of the turbulent fluxes (Burchard, 2002). For the discrete values, not to interfere with the grid indices, the subscript p for the plume quantities is now a superscript such that plume quantities are now noted $X^p_{j+1/2} = X_p(z = z_{j+1/2})$. In the following, we consider that the plume quantities and k are discretized at cell interfaces and the mean quantities $\overline{X}$ are discretized at cell centers and are interpreted in a finite-volume sense (i.e. $\overline{X}_j = \dfrac{1}{\Delta z_j} \displaystyle\int_{z_{j-1/2}}^{z_{j+1/2}} \overline{X}(z)\, {\rm d}z$). In the remainder, we consider the oceanic case with $\sigma_o^a = -1$.

F1 Discretization of mass-flux equations

We consider here the mass-flux equations given in Tab. 1 but in conservative form (except for the vertical velocity and TKE plume equations) :

$$\partial_z(a_p w_p) = E - D \tag{F1}$$
$$\partial_z(a_p w_p \phi_p) = E\overline{\phi} - D\phi_p \tag{F2}$$
$$\partial_z(a_p w_p \boldsymbol{U}_p) = E\overline{\boldsymbol{U}} - D\boldsymbol{U}_p \tag{F3}$$
$$w_p \partial_z w_p = -(E/a_p)(b w_p) + aB_p + b' w_p^2 \tag{F4}$$
$$a_p w_p \partial_z k_p = E\left(k - k_p + \frac{1}{2}(\overline{\boldsymbol{u}}_p - \overline{\boldsymbol{u}})^2\right) - a_p(\epsilon_\nu)_p \tag{F5}$$

where the equation for horizontal momentum has been manipulated to have the same form as the ϕ_p equation by taking $\boldsymbol{U}_p = \boldsymbol{u}_{h,p} - C_u\overline{\boldsymbol{u}}_h$ and $\overline{\boldsymbol{U}} = (1 - C_u)\overline{\boldsymbol{u}}_h$. The advective form is used for the w_p equation to make the computation of w_p independent of a_p (with the closure hypothesis (25) for E, E/a_p is independent of a_p); the motivations for this will become clearer later. The mass-flux equations correspond to a first-order nonlinear set of ODEs. There are a whole lot of methods for solving such initial value problems. We present here a simple method combining explicit (Euler) and semi-implicit (Crank-Nicolson) steps as the use of more advanced methods did not produce significantly different results. In the following, we describe the different steps for the resolution starting from known initial values $X^p_{N+1/2}$ at the surface and advancing downward.

F11 Initial conditions

The discrete form of the initial conditions given in 2.4 are obtained by a linear extrapolation of $\overline{\phi}_N$ and $(\overline{\boldsymbol{u}}_h)_N$ toward the surface.

$$\begin{aligned} w^p_{N+1/2} &= -w^p_{\min} \\ \phi^p_{N+1/2} &= \frac{(2\Delta z_N + \Delta z_{N-1})\overline{\phi}_N - \Delta z_N \overline{\phi}_{N-1}}{\Delta z_N + \Delta z_{N-1}} \\ \boldsymbol{U}^p_{N+1/2} &= (1 - C_u)\frac{(2\Delta z_N + \Delta z_{N-1})(\overline{\boldsymbol{u}}_h)_N - \Delta z_N(\overline{\boldsymbol{u}}_h)_{N-1}}{\Delta z_N + \Delta z_{N-1}} \end{aligned} \tag{F6}$$

Since the TKE k is already discretized at cell interfaces the boundary condition for k_p does not require an extrapolation. In particular the condition on ϕ_p leads to the following value of the B_p term in the topmost grid cell :

$$B^p_N = \Delta z_N \left(\frac{\overline{b}_N - \overline{b}_{N-1}}{\Delta z_N + \Delta z_{N-1}}\right) = \frac{\Delta z_N}{2}\left(N^2\right)_{N-1/2}$$

meaning that using the condition (F6) allows to trigger convection as soon as the Brunt-Väisälä frequency is negative. Indeed a negative value of B^p_N in the RHS of the w_p-equation (F4) leads to a positive value of $(\partial_z w_p)_N$ and thus larger negative values of w_p when going downward.

F12 w_p-equation

The w_p-equation (F4) using the entrainment E given in (25) can be formulated as

$$\partial_z w_p^2 + b\beta_1 \min(\partial_z w_p^2, 0) = 2aB_p + 2b' w_p^2$$

which can be discretized in a straightforward way as

$$\begin{aligned} \widetilde{\beta}\left[(w^p)^2_{j+1/2} - (w^p)^2_{j-1/2}\right] &= 2a\Delta z_j B^p_j - \sigma^a_o(b'\Delta z_j)\left[(w^p)^2_{j+1/2} + (w^p)^2_{j-1/2}\right] \\ B^p_j &= b_{\text{eos}}(\phi^p_{j+1/2}) - b_{\text{eos}}(\overline{\phi}_j) \end{aligned} \tag{F7}$$

where $\widetilde{\beta} = 1 + b\beta_1$ if $aB_j^p - \sigma_o^a b'(w^p)_{j+1/2}^2$ is negative and $\widetilde{\beta} = 1$ otherwise. Knowing $w_{j+1/2}^p$, it is easily found that

$$(w^p)_{j-1/2}^2 = \frac{(\widetilde{\beta} - b'\Delta z_j)(w^p)_{j+1/2}^2 - 2a\Delta z_j B_j^p}{\widetilde{\beta} + b'\Delta z_j}$$

Once this quantity falls below a certain threshold $(w_{\min}^p)^2$, the plume is considered evanescent. In the oceanic context we consider $w_{j-1/2}^p = -\sqrt{(w^p)_{j-1/2}^2}$ for the rest of the calculations to guarantee that $w_{j-1/2}^p$ is strictly negative. The upwinding used to compute B_p in (F7) in addition to the fact that the w_p-equation does not depend on a_p avoid the need for an iterative process to solve the mass-flux equations.

F13 Continuity and tracer equations

The entrainment E_j and detrainment D_j rates given in (25) and (26) discretized on a grid cell j correspond to

$$\begin{aligned}
\Delta z_j E_j &= \frac{1}{2}\left(a_{j+1/2}^p + a_{j-1/2}^p\right)\beta_1(\delta_z w^p)_j^+ \\
\Delta z_j D_j &= \frac{1}{2}\left(a_{j+1/2}^p + a_{j-1/2}^p\right)\left[-\beta_2(\delta_z w^p)_j^- - \frac{\delta_0 \Delta z_j}{2}(w_{j+1/2}^p + w_{j-1/2}^p)\right]
\end{aligned}$$

where $(\delta_z w^p)_j^+ = \max\left(w_{j+1/2}^p - w_{j-1/2}^p, 0\right)$ and $(\delta_z w^p)_j^- = \min\left(w_{j+1/2}^p - w_{j-1/2}^p, 0\right)$. Integrating from $z_{j-1/2}$ to $z_{j+1/2}$ the continuity equation and ϕ_p equations we obtain

$$\begin{aligned}
(a^p w^p)_{j+1/2} - (a^p w^p)_{j-1/2} &= \Delta z_j (E_j - D_j) \\
(a^p w^p \phi^p)_{j+1/2} - (a^p w^p \phi^p)_{j-1/2} &= \Delta z_j E_j \overline{\phi}_j - (\Delta z_j D_j/2)\left(\phi_{j+1/2}^p + \phi_{j-1/2}^p\right)
\end{aligned}$$

which can also be extended to the horizontal momentum equation formulated using $\boldsymbol{U}_p$. Since at this stage $w_{j+1/2}^p$ and $w_{j-1/2}^p$ are known, the continuity equation is used to compute $a_{j-1/2}^p$ through

$$\begin{aligned}
a_{j-1/2}^p &= a_{j+1/2}^p \left\{\frac{2w_{j+1/2}^p - \mathrm{EmD}_j}{2w_{j-1/2}^p + \mathrm{EmD}_j}\right\} \\
\mathrm{EmD}_j &= \beta_1(\delta_z w^p)_j^+ + \beta_2(\delta_z w^p)_j^- + \min\left\{\frac{\delta_0 \Delta z_j}{2}(w_{j+1/2}^p + w_{j-1/2}^p), -2(w_{\min}^p)\right\}
\end{aligned} \tag{F8}$$

Note that a_p is subject to a boundedness requirement as $0 \leq a_p \leq 1$. Assuming $0 \leq a_{j+1/2}^p \leq 1$, sufficient conditions to guarantee that $a_{j-1/2}^p \leq 1$ are $\beta_1 \leq 1$ and $\beta_2 \geq 1$ and a sufficient condition to guarantee that $a_{j-1/2}^p \geq 0$ is $\beta_2 < 2$. Moreover a constraint is added on the background detrainment δ_0 in (F8) to guarantee that $a_{j-1/2}^p = 0$ as soon as $w_{j+1/2}^p = w_{j-1/2}^p = -w_{\min}^p$ which occurs once outside the plume.

Once $a_{j-1/2}^p$ is known, it is possible to compute $\phi_{j-1/2}^p$ (as well as $\boldsymbol{U}_{j-1/2}^p$). The proposed discretization ensures that the compatibility between the continuity and the tracer equations is maintained at the discrete level (*i.e.* we recover the continuity equation for $\phi_{j+1/2}^p = \phi_{j-1/2}^p = 1$ and $\overline{\phi}_j = 1$).

The same reasoning can be applied to solve the k_p equation, which presents no additional difficulties as all necessary quantities $w_{j\pm1/2}^p$, $a_{j\pm1/2}^p$ and $\boldsymbol{u}_{j\pm1/2}^p$ are known.

In summary, the proposed discretization guarantees that w_p is strictly negative, that a_p is bounded between 0 and 1, and that the continuity and tracer equations are compatible, without the need for an iterative solution procedure.

F2 Energy consistent discretization of turbulent kinetic energy

In Burchard (2002) an energetically consistent discretization of the turbulent shear and buoyancy production terms for the TKE equation in the ED case is derived. Such methodology can be extended in the EDMF case to discretize the MF-related TKE production terms given in magenta and cyan in Tab. 2. Starting from a simple Euler-upwind discretization of mass-flux terms in the $\overline{\boldsymbol{u}}_h$ and $\overline{\phi}$ equations which can be written generically for a variable X

$$\frac{\overline{X}_j^{n+1}-\overline{X}_j^n}{\Delta t}=\frac{F^{\mathrm{MF}}_{j+1/2}-F^{\mathrm{MF}}_{j-1/2}}{\Delta z_j}$$
$$F^{\mathrm{MF}}_{j+1/2}=(a^p w^p)_{j+1/2}\left(\overline{X}^p_{j+1/2}-\overline{X}^n_j\right)$$

the kinetic and potential energy budgets can be derived by multiplying the velocity equations (*i.e.* $\overline{X}=u$) by $(\overline{u}_j^{n+1}+\overline{u}_j^n)/2$ and the buoyancy equation by $-z_j$. After some simple algebra, we obtain that

$$(a_p w_p(\boldsymbol{u}_{h,p}-\overline{\boldsymbol{u}}_h)\cdot\partial_z\overline{\boldsymbol{u}}_h)_{j+1/2}=(a_pw_p)_{j+1/2}\left((\boldsymbol{u}_h)^p_{j+1/2}-(\boldsymbol{u}_h)^n_j\right)\cdot\left(\frac{(\boldsymbol{u}_h)^{n+1}_{j+1}+(\boldsymbol{u}_h)^n_{j+1}-(\boldsymbol{u}_h)^{n+1}_j-(\boldsymbol{u}_h)^n_j}{2\Delta z_{j+1/2}}\right)$$
$$\left(a_pw_p(b_p-\bar{b})\right)_{j+1/2}=(a_pw_p)_{j+1/2}B^p_j$$

where B^p_j is given in (F7). Using these discrete forms for the MF-related TKE production terms combined with the discretization of the turbulent shear and buoyancy production terms derived in Burchard (2002) ensure the proper energy flux between resolved and subgrid energies.

F3 Coupling ED and MF schemes

In the EDMF approach, the usual vertical diffusion/viscous subgrid terms are completed by an advective term so that the following equation must be advanced in time:

$$\partial_t\overline{X}=\partial_z\left(K_X\partial_z\overline{X}\right)-\partial_z\left(a_pw_p(X^p-\overline{X})\right) \tag{F9}$$

This amounts to couple a boundary layer scheme which provides K_X and a convection scheme which provides a_pw_p and X^p. The numerical treatment of such coupling is rarely discussed in the literature. This problem can be approached in 2 ways: either by integrating the 2 schemes sequentially or in parallel. For the numerical experiments discussed in Sec. 5 we chose a *boundary layer-then-convection* strategy corresponding to the following temporal integration for the single-column model (leaving aside the Coriolis and solar penetration terms)

ED step
$$\phi^{n+1,\star}=\phi^n+\Delta t\partial_z\left(K_\phi(k^n,b^n)\partial_z\phi^{n+1,\star}\right)$$
$$\boldsymbol{u}_h^{n+1,\star}=\boldsymbol{u}_h^n+\Delta t\partial_z\left(K_{\boldsymbol{u}}(k^n,b^n)\partial_z\boldsymbol{u}_h^{n+1,\star}\right)$$
$$b^{n+1,\star}=b_{\mathrm{eos}}(\phi^{n+1,\star})$$
MF step
$$[a_p,w_p,\phi_p,\boldsymbol{u}_{h,p},k_p,B_p]=\mathrm{MF}(b^{n+1,\star},\boldsymbol{u}_h^{n+1,\star})$$
$$\phi^{n+1}=\phi^{n+1,\star}-\Delta t\partial_z\left(a_pw_p(\phi_p-\phi^{n+1,\star})\right)$$
$$\boldsymbol{u}_h^{n+1}=\boldsymbol{u}_h^{n+1,\star}-\Delta t\partial_z\left(a_pw_p(\boldsymbol{u}_{h,p}-\boldsymbol{u}_h^{n+1,\star})\right)$$
TKE update
$$k^{n+1}=k^n+\Delta t\partial_z\left(K_k(k^n,b^n)\partial_zk^{n+1}\right)+\mathcal{F}_k(b^{n+1},\boldsymbol{u}_h^{n+1},\boldsymbol{u}_h^n,a_p,w_p,\boldsymbol{u}_{h,p},k_p,B_p)$$

where the MF(.) function represents the computation of mass-flux quantities as described previously and $\mathcal{F}_k$ contains the TKE transport and forcing terms. The "ED step" is clas-

sically computed using an Euler backward scheme. With the proposed approach, the convection scheme sees a state already updated by the boundary layer scheme (and by the solar penetration and non-solar surface heat flux which are applied during the "ED step") The convection scheme thus sees a state whose static stability is representative of the current time-step and external forcing.

Ultimately, with the proposed approach, the various stages can be expressed directly as follows

$$\begin{aligned}\phi^{n+1} &= \phi^n + \Delta t \partial_z \left(K_\phi \partial_z \phi^{n+1,\star} - a_p w_p (\phi_p - \phi^{n+1,\star}) \right) \\ [a_p, w_p, \phi_p] &= \mathrm{MF}(\phi^{n+1,\star})\end{aligned}$$

which reflects the fact that we have good synchronization between the ED part and the MF part, which see the same mean fields. On the other hand, the approach of simultaneously considering the ED and MF parts in a single tridiagonal problem would lead to

$$\begin{aligned}\phi^{n+1} &= \phi^n + \Delta t \left(K_\phi \partial_z \phi^{n+1} - a_p w_p (\phi_p - \phi^{n+1}) \right) \\ [a_p, w_p, \phi_p] &= \mathrm{MF}(\phi^n)\end{aligned}$$

In this case, the mass flux is applied to the mean fields at time n thus breaking the synchronization between the ED and MF parts. Indeed ϕ_p has been computed using ϕ^n while it is applied at time $n+1$.

Open Research

Data Availability Statement

Data from the Lion mooring (located in the Gulf of Lion; Mediterranean sea) are freely accessible from Bosse et al. (2023). The output from LES simulations and the initial and surface boundary conditions for the Hymex/ASICS-MED experiments are available at Zenodo link here.

Software Availability Statement

All the numerical codes used in this study have been made available and can be found at Zenodo link here. It includes the single-column model with Eddy-Diffusivity Mass-Flux turbulent closure developed from scratch. The latter consists of low-level code written in Fortran interfaced with Python using F2PY (Peterson, 2009). The single-column simulations analyzed in this study can be executed from a high-level Python driver code without any intervention on the Fortran code. The high-level Python driver code and scripts to reproduce the figures are available in the Zenodo archive. The Fortran code contains inline documentation following the FORD (Fortran Documenter) format.

Acknowledgments

This work was supported by the *institut des Mathématiques pour la Planète Terre* (iMPT) through the project "Coherent sub-grid scale modeling for ocean climate models". This study was carried out as part of the technological defense project PROTEVS2 under the auspices of the French Ministry of the Armies / DGA. MP was supported by a PhD fellowship from Ecole Normale Supérieure Paris. The authors are extremely grateful to Jean-Luc Redelsperger for his essential contributions to the MESO-NH model and Thomas Dubos for constructive comments on an earlier version of this paper. This research was funded in part by l'Agence Nationale de la Recherche (ANR), project ANR-23-CE01-0009.

References

Arakawa, A., & Schubert, W. H. (1974). Interaction of a Cumulus Cloud Ensemble with the Large-Scale Environment, Part I. *J. Atmos. Sci.*, *31*(3), 674–701. doi: 10.1175/1520-0469(1974)031⟨0674:IOACCE⟩2.0.CO;2

Bony, S., Stevens, B., Frierson, D. M. W., Jakob, C., Kageyama, M., Pincus, R., ... Webb, M. J. (2015). Clouds, circulation and climate sensitivity. *Nat. Geosci.*, *8*(4), 261–268. doi: 10.1038/ngeo2398

Bosse, A., Testor, P., Coppola, L., Bretel, P., Dausse, D., Durrieu de Madron, X., ... D'ortenzio, F. (2023). *LION observatory data.* Retrieved from `https://doi.org/10.17882/44411` (Type: Dataset) doi: 10.17882/44411

Bretherton, C. S., McCaa, J. R., & Grenier, H. (2004, April). A New Parameterization for Shallow Cumulus Convection and Its Application to Marine Subtropical Cloud-Topped Boundary Layers. Part I: Description and 1D Results. *Monthly Weather Review*, *132*(4), 864–882. Retrieved from `https://journals.ametsoc.org/view/journals/mwre/132/4/1520-0493_2004_132_0864_anpfsc_2.0.co_2.xml` doi: 10.1175/1520-0493(2004)132⟨0864:ANPFSC⟩2.0.CO;2

Brient, F., Couvreux, F., Rio, C., & Honnert, R. (2023). Coherent subsiding structures in large eddy simulations of atmospheric boundary layers. *Quart. J. Roy. Meteorol. Soc.*. doi: 10.1002/qj.4625

Burchard, H. (2002). Energy-conserving discretisation of turbulent shear and buoyancy production. *Ocean Modell.*, *4*(3-4), 347–361. doi: 10.1016/S1463-5003(02)00009-4

Coppola, L., Prieur, L., Taupier-Letage, I., Estournel, C., Testor, P., Lefevre, D., ... Taillandier, V. (2017). Observation of oxygen ventilation into deep waters through targeted deployment of multiple argo-o2 floats in the northwestern mediterranean sea in 2013. *J. Geophys. Res.*, *122*(8), 6325-6341. doi: https://doi.org/10.1002/2016JC012594

Couvreux, F., Guichard, F., Masson, V., & Redelsperger, J.-L. (2007). Negative water vapour skewness and dry tongues in the convective boundary layer: observations and large-eddy simulation budget analysis. *Bound.-Lay. Meteorol.*, *123*(2), 269–294. doi: 10.1007/s10546-006-9140-y

Couvreux, F., Hourdin, F., & Rio, C. (2010, March). Resolved Versus Parametrized Boundary-Layer Plumes. Part I: A Parametrization-Oriented Conditional Sampling in Large-Eddy Simulations. *Boundary-Layer Meteorology*, *134*(3), 441–458. Retrieved 2022-02-21, from `https://doi.org/10.1007/s10546-009-9456-5` doi: 10.1007/s10546-009-9456-5

Couvreux, F., Hourdin, F., Williamson, D., Roehrig, R., Volodina, V., Villefranque, N., ... Xu, W. (2021). Process-Based Climate Model Development Harnessing Machine Learning: I. A Calibration Tool for Parameterization Improvement. *J. Adv. Model. Earth Syst.*, *13*(3), e2020MS002217. doi: 10.1029/2020MS002217

Craig, P. D., & Banner, M. L. (1994). Modeling Wave-Enhanced Turbulence in the Ocean Surface Layer. *J. Phys. Oceanogr.*, *24*(12), 2546–2559. doi: 10.1175/1520-0485(1994)024⟨2546:MWETIT⟩2.0.CO;2

Cuxart, J., Bougeault, P., & Redelsperger, J.-L. (2000). A turbulence scheme allowing for mesoscale and large-eddy simulations. *Quart. J. Roy. Meteorol. Soc.*, *126*(562), 1–30. doi: 10.1002/qj.49712656202

Deardorff, J. W. (1966). The Counter-Gradient Heat Flux in the Lower Atmosphere and in the Laboratory. *J. Atmos. Sci.*, *23*(5), 503–506. doi: 10.1175/1520-0469(1966)023⟨0503:TCGHFI⟩2.0.CO;2

Deardorff, J. W. (1970). Convective Velocity and Temperature Scales for the Unstable Planetary Boundary Layer and for Rayleigh Convection. *J. Atmos. Sci.*, *27*(8), 1211–1213. doi: 10.1175/1520-0469(1970)027⟨1211:CVATSF⟩2.0.CO;2

Denbo, D. W., & Skyllingstad, E. D. (1996). An ocean large-eddy simulation model with application to deep convection in the Greenland Sea. *J. Geophys. Res.*,

101(C1), 1095–1110. doi: 10.1029/95JC02828

de Rooy, W. C., Bechtold, P., Fröhlich, K., Hohenegger, C., Jonker, H., Mironov, D., ... Yano, J.-I. (2013). Entrainment and detrainment in cumulus convection: an overview. *Quart. J. Roy. Meteorol. Soc.*, *139*(670), 1–19. doi: 10.1002/qj.1959

Eden, C. (2016). Closing the energy cycle in an ocean model. *Ocean Modell.*, *101*, 30–42. doi: 10.1016/j.ocemod.2016.02.005

Eden, C., & Olbers, D. (2014). An Energy Compartment Model for Propagation, Nonlinear Interaction, and Dissipation of Internal Gravity Waves. *J. Phys. Oceanogr.*, *44*(8), 2093–2106. doi: 10.1175/JPO-D-13-0224.1

Eldred, C., & Gay-Balmaz, F. (2021). Thermodynamically consistent semi-compressible fluids: a variational perspective. *J. Phys. A Math. Theor.*, *54*, 345701. doi: 10.1088/1751-8121/ac1384

Evans, L. C. (2010). *Partial Differential Equations*. American Mathematical Soc.

Fox-Kemper, B., Adcroft, A., Böning, C. W., Chassignet, E. P., Curchitser, E., Danabasoglu, G., ... Yeager, S. G. (2019). Challenges and Prospects in Ocean Circulation Models. *Front. Mar. Sci.*, *6*, 65. doi: 10.3389/fmars.2019.00065

Garanaik, A., Pereira, F. S., Smith, K., Robey, R., Li, Q., Pearson, B., & Van Roekel, L. (2024). A New Hybrid Mass-Flux/High-Order Turbulence Closure for Ocean Vertical Mixing. *Journal of Advances in Modeling Earth Systems*, *16*(1). Retrieved 2024-01-31, from `https://onlinelibrary.wiley.com/doi/abs/10.1029/2023MS003846` (_eprint: https://onlinelibrary.wiley.com/doi/pdf/10.1029/2023MS003846) doi: 10.1029/2023MS003846

Garcia, J. R., & Mellado, J. P. (2014). The Two-Layer Structure of the Entrainment Zone in the Convective Boundary Layer. *J. Atmos. Sci.*, *71*(6), 1935–1955. doi: 10.1175/JAS-D-13-0148.1

Garratt, J. (1994a). *The Atmospheric Boundary Layer*. Cambridge University Press.

Garratt, J. (1994b). Review: the atmospheric boundary layer. *Earth-Science Reviews*, *37*(1-2), 89–134. doi: 10.1016/0012-8252(94)90026-4

Gaspar, P., Grégoris, Y., & Lefevre, J.-M. (1990). A simple eddy kinetic energy model for simulations of the oceanic vertical mixing: Tests at station Papa and long-term upper ocean study site. *J. Geophys. Res.*, *95*(C9), 16179–16193. doi: 10.1029/JC095iC09p16179

Giordani, H., Bourdallé-Badie, R., & Madec, G. (2020). An Eddy-Diffusivity Mass-Flux Parameterization for Modeling Oceanic Convection. *J. Adv. Model. Earth Syst.*, *12*. doi: 10.1029/2020MS002078

Gregory, D., Kershaw, R., & Inness, P. M. (1997). Parametrization of momentum transport by convection. II: Tests in single-column and general circulation models. *Quart. J. Roy. Meteorol. Soc.*, *123*(541), 1153–1183. doi: 10.1002/qj.49712354103

Haghshenas, A., & Mellado, J. P. (2019). Characterization of wind-shear effects on entrainment in a convective boundary layer. *J. Fluid Mech.*, *858*, 145–183. doi: 10.1017/jfm.2018.761

Hahn, D. W., & Özişik, M. N. (2012). *Heat Conduction* (1st ed.). Wiley. doi: 10.1002/9781118411285

Han, J., & Bretherton, C. S. (2019). TKE-Based Moist Eddy-Diffusivity Mass-Flux (EDMF) Parameterization for Vertical Turbulent Mixing. *Weather Forecast.*, *34*(4), 869–886. doi: 10.1175/WAF-D-18-0146.1

Higgins, C. W., Katul, G. G., Froidevaux, M., Simeonov, V., & Parlange, M. B. (2013). Are atmospheric surface layer flows ergodic? *Geophys. Res. Lett.*, *40*(12), 3342–3346.

Holtslag, A. A. M., & Moeng, C.-H. (1991). Eddy diffusivity and countergradient transport in the convective atmospheric boundary layer. *J. Atmos. Sci.*,

48(14), 1690 - 1698. doi: https://doi.org/10.1175/1520-0469(1991)048⟨1690:EDACTI⟩2.0.CO;2

Honnert, R., Couvreux, F., Masson, V., & Lancz, D. (2016). Sampling the Structure of Convective Turbulence and Implications for Grey-Zone Parametrizations. *Bound.-Lay. Meteorol.*, *160*(1), 133–156. doi: 10.1007/s10546-016-0130-4

Hourdin, F., Couvreux, F., & Menut, L. (2002). Parameterization of the Dry Convective Boundary Layer Based on a Mass Flux Representation of Thermals. *J. Atmos. Sci.*, *59*(6), 1105–1123. doi: 10.1175/1520-0469(2002)059⟨1105:POTDCB⟩2.0.CO;2

Hourdin, F., Mauritsen, T., Gettelman, A., Golaz, J.-C., Balaji, V., Duan, Q., ... Williamson, D. (2017). The Art and Science of Climate Model Tuning. *Bull. Amer. Meteor. Soc.*, *98*(3), 589–602. doi: 10.1175/BAMS-D-15-00135.1

Jansen, M. F., Adcroft, A., Khani, S., & Kong, H. (2019). Toward an Energetically Consistent, Resolution Aware Parameterization of Ocean Mesoscale Eddies. *J. Adv. Model. Earth Syst.*, *11*(8), 2844–2860. doi: 10.1029/2019MS001750

Johansson, C., Smedman, A.-S., Högström, U., Brasseur, J. G., & Khanna, S. (2001). Critical Test of the Validity of Monin–Obukhov Similarity during Convective Conditions. *J. Atmos. Sci.*, *58*(12), 1549–1566. doi: 10.1175/1520-0469(2001)058⟨1549:CTOTVO⟩2.0.CO;2

Kato, H., & Phillips, O. M. (1969). On the penetration of a turbulent layer into stratified fluid. *J. Fluid Mech.*, *37*(4), 643–655. doi: 10.1017/S0022112069000784

Lac, C., Chaboureau, J.-P., Masson, V., Pinty, J.-P., Tulet, P., Escobar, J., ... Wautelet, P. (2018). Overview of the Meso-NH model version 5.4 and its applications. *Geosci. Model Dev.*, *11*(5), 1929–1969. doi: 10.5194/gmd-11-1929-2018

Large, W. G., McWilliams, J. C., & Doney, S. C. (1994). Oceanic vertical mixing: A review and a model with a nonlocal boundary layer parameterization. *Rev. Geophys.*, *32*(4), 363–403. doi: 10.1029/94RG01872

Lauritzen, P. H., Kevlahan, N. K.-R., Toniazzo, T., Eldred, C., Dubos, T., Gassmann, A., ... Bacmeister, J. T. (2022). Reconciling and Improving Formulations for Thermodynamics and Conservation Principles in Earth System Models (ESMs). *J. Adv. Model. Earth Syst.*, *14*(9), e2022MS003117. doi: 10.1029/2022MS003117

Legay, A., Deremble, B., Penduff, T., Brasseur, P., & Molines, J.-M. (2023). *A generic framework for evaluating the oceanic mixed layer depth dynamics* (preprint). Preprints. doi: 10.22541/essoar.168563421.17506622/v1

LeVeque, R. J. (2002). *Finite volume methods for hyperbolic problems* (Vol. 31). Cambridge university press.

Li, Q., Cheng, Y., & Gentine, P. (2021). Connection Between Mass Flux Transport and Eddy Diffusivity in Convective Atmospheric Boundary Layers. *Geophys. Res. Lett.*, *48*(8), e2020GL092073. doi: 10.1029/2020GL092073

Li, Q., Gentine, P., Mellado, J. P., & McColl, K. A. (2018). Implications of Nonlocal Transport and Conditionally Averaged Statistics on Monin–Obukhov Similarity Theory and Townsend's Attached Eddy Hypothesis. *J. Atmos. Sci.*, *75*(10), 3403–3431. doi: 10.1175/JAS-D-17-0301.1

Madec, G., Bourdallé-Badie, R., Chanut, J., Clementi, E., Coward, A., Ethé, C., ... Samson, G. (2019). *NEMO ocean engine.* Retrieved from `https://zenodo.org/record/1464816` doi: 10.5281/ZENODO.1464816

Madec, G., Delecluse, P., Crepon, M., & Chartier, M. (1991). A Three-Dimensional Numerical Study of Deep-Water Formation in the Northwestern Mediterranean Sea. *J. Phys. Oceanogr.*, *21*(9), 1349–1371. doi: 10.1175/1520-0485(1991)021⟨1349:ATDNSO⟩2.0.CO;2

Marshall, J., Hill, C., Perelman, L., & Adcroft, A. (1997). Hydrostatic, quasi-hydrostatic, and nonhydrostatic ocean modeling. *J. Geophys. Res.*, *102*(C3),

5733–5752. doi: 10.1029/96JC02776

Marshall, J., & Schott, F. (1999). Open-ocean convection: Observations, theory, and models. *Rev. Geophys.*, *37*(1), 1–64. doi: 10.1029/98RG02739

Martin, T., Park, W., & Latif, M. (2013). Multi-centennial variability controlled by Southern Ocean convection in the Kiel Climate Model. *Clim. Dynam.*, *40*(7), 2005–2022. doi: 10.1007/s00382-012-1586-7

McDougall, T. J. (2003). Potential Enthalpy: A Conservative Oceanic Variable for Evaluating Heat Content and Heat Fluxes. *J. Phys. Oceanogr.*, *33*(5), 945–963. doi: 10.1175/1520-0485(2003)033⟨0945:PEACOV⟩2.0.CO;2

Mellor, G. (1973). Analytic Prediction of the Properties of Stratified Planetary Surface Layers. *J. Atmos. Sci.*, *30*(6), 1061–1069. doi: 10.1175/1520-0469(1973)030⟨1061:APOTPO⟩2.0.CO;2

Mellor, G., & Blumberg, A. (2004). Wave Breaking and Ocean Surface Layer Thermal Response. *J. Phys. Oceanogr.*, *34*(3), 693–698. doi: 10.1175/2517.1

Moore, G. W. K., Våge, K., Pickart, R. S., & Renfrew, I. A. (2015). Decreasing intensity of open-ocean convection in the Greenland and Iceland seas. *Nat. Clim. Change*, *5*(9), 877–882. doi: 10.1038/nclimate2688

Obukhov, A. M. (1971). Turbulence in an atmosphere with a non-uniform temperature. *Bound.-Lay. Meteorol.*, *2*(1), 7–29. doi: 10.1007/BF00718085

Olbers, D., Willebrand, J., & Eden, C. (2012). *Ocean Dynamics*. Berlin, Heidelberg: Springer Berlin Heidelberg. doi: 10.1007/978-3-642-23450-7

Pauluis, O. (2008). Thermodynamic Consistency of the Anelastic Approximation for a Moist Atmosphere. *J. Atmos. Sci.*, *65*, 2719–2729. doi: 10.1175/2007JAS2475.1

Pergaud, J., Masson, V., Malardel, S., & Couvreux, F. (2009). A Parameterization of Dry Thermals and Shallow Cumuli for Mesoscale Numerical Weather Prediction. *Bound.-Lay. Meteorol.*, *132*, 83–106. doi: 10.1007/s10546-009-9388-0

Peterson, P. (2009). F2PY: a tool for connecting Fortran and Python programs. *Int. j. comput. sci. eng.*, *4*(4), 296. doi: 10.1504/IJCSE.2009.029165

Piron, A., Thierry, V., Mercier, H., & Caniaux, G. (2016). Argo float observations of basin-scale deep convection in the Irminger sea during winter 2011–2012. *Deep-Sea Res. I*, *109*, 76–90. doi: 10.1016/j.dsr.2015.12.012

Pope, S. B. (2004). Ten questions concerning the large-eddy simulation of turbulent flows. *New J. Phys.*, *6*, 35–35. doi: 10.1088/1367-2630/6/1/035

Ramadhan, A., Wagner, G. L., Hill, C., Campin, J.-M., Churavy, V., Besard, T., ... Marshall, J. (2020). Oceananigans.jl: Fast and friendly geophysical fluid dynamics on GPUs. *Journal of Open Source Software*, *5*(53), 2018. Retrieved from `https://doi.org/10.21105/joss.02018` doi: 10.21105/joss.02018

Resseguier, V., Mémin, E., & Chapron, B. (2017). Geophysical flows under location uncertainty, Part II Quasi-geostrophy and efficient ensemble spreading. *Geophys. Astrophys. Fluid Dyn.*, *111*(3), 177–208.

Rio, C., Hourdin, F., Couvreux, F., & Jam, A. (2010). Resolved Versus Parametrized Boundary-Layer Plumes. Part II: Continuous Formulations of Mixing Rates for Mass-Flux Schemes. *Bound.-Lay. Meteorol.*, *135*(3), 469–483. doi: 10.1007/s10546-010-9478-z

Roode, S. R. d., Siebesma, A. P., Jonker, H. J. J., & Voogd, Y. d. (2012). Parameterization of the Vertical Velocity Equation for Shallow Cumulus Clouds. *Mon. Weather Rev.*, *140*(8), 2424–2436. doi: 10.1175/MWR-D-11-00277.1

Rotunno, R., & Klemp, J. B. (1982). The Influence of the Shear-Induced Pressure Gradient on Thunderstorm Motion. *Mon. Weather Rev.*, *110*(2), 136–151. doi: 10.1175/1520-0493(1982)110⟨0136:TIOTSI⟩2.0.CO;2

Schmidt, H., & Schumann, U. (1989). Coherent structure of the convective boundary layer derived from large-eddy simulations. *J. Fluid Mech.*, *200*, 511–562. doi: 10.1017/S0022112089000753

Schmitt, F. G. (2007). About Boussinesq's turbulent viscosity hypothesis: histori-

cal remarks and a direct evaluation of its validity. *Comptes Rendus Mécanique*, *335*(9), 617–627. doi: 10.1016/j.crme.2007.08.004

Schneider, T., Teixeira, J., Bretherton, C. S., Brient, F., Pressel, K. G., Schär, C., & Siebesma, A. P. (2017). Climate goals and computing the future of clouds. *Nat. Clim. Change*, *7*(1), 3–5. doi: 10.1038/nclimate3190

Siebesma, A. P., Soares, P. M. M., & Teixeira, J. (2007). A Combined Eddy-Diffusivity Mass-Flux Approach for the Convective Boundary Layer. *J. Atmos. Sci.*, *64*(4), 1230–1248. doi: 10.1175/JAS3888.1

Soares, P. M. M., Miranda, P. M. A., Siebesma, A. P., & Teixeira, J. (2004). An eddy-diffusivity/mass-flux parametrization for dry and shallow cumulus convection. *Quart. J. Roy. Meteorol. Soc.*, *130*(604), 3365–3383. doi: 10.1256/qj.03.223

Souza, A. N., Wagner, G. L., Ramadhan, A., Allen, B., Churavy, V., Schloss, J., ... Ferrari, R. (2020). Uncertainty Quantification of Ocean Parameterizations: Application to the K-Profile-Parameterization for Penetrative Convection. *J. Adv. Model. Earth Syst.*, *12*(12). doi: 10.1029/2020MS002108

Tailleux, R. (2012). Thermodynamics/Dynamics Coupling in Weakly Compressible Turbulent Stratified Fluids. *International Scholarly Research Notices*, *2012*, e609701. (Publisher: Hindawi) doi: 10.5402/2012/609701

Tailleux, R., & Dubos, T. (2023). *A Simple and Transparent Method for Improving the Energetics and Thermodynamics of Seawater Approximations: Static Energy Asymptotics (SEA).* arXiv. (arXiv:2311.11387 [physics]) doi: 10.48550/arXiv.2311.11387

Tan, Z., Kaul, C. M., Pressel, K. G., Cohen, Y., Schneider, T., & Teixeira, J. (2018). An Extended Eddy-Diffusivity Mass-Flux Scheme for Unified Representation of Subgrid-Scale Turbulence and Convection. *J. Adv. Model. Earth Syst.*, *10*(3), 770–800. doi: 10.1002/2017MS001162

Thuburn, J., Weller, H., Vallis, G. K., Beare, R. J., & Whitall, M. (2018). A Framework for Convection and Boundary Layer Parameterization Derived from Conditional Filtering. *J. Atmos. Sci.*, *75*(3), 965–981. doi: 10.1175/JAS-D-17-0130.1

Troen, I. B., & Mahrt, L. (1986). A simple model of the atmospheric boundary layer; sensitivity to surface evaporation. *Bound.-Lay. Meteorol.*, *37*(1), 129–148. doi: 10.1007/BF00122760

Turner, J. S. (1979). *Buoyancy Effects in Fluids.* Cambridge University Press.

Vallis, G. K. (2017). *Atmospheric and oceanic fluid dynamics.* Cambridge University Press.

Van Roekel, L., Adcroft, A. J., Danabasoglu, G., Griffies, S. M., Kauffman, B., Large, W., ... Schmidt, M. (2018). The KPP Boundary Layer Scheme for the Ocean: Revisiting Its Formulation and Benchmarking One-Dimensional Simulations Relative to LES. *J. Adv. Model. Earth Syst.*, *10*(11), 2647–2685. doi: 10.1029/2018MS001336

Waldman, R., Somot, S., Herrmann, M., Bosse, A., Caniaux, G., Estournel, C., ... Testor, P. (2017). Modeling the intense 2012-2013 dense water formation event in the northwestern mediterranean sea: Evaluation with an ensemble simulation approach. *J. Geophys. Res.*, *122*(2), 1297-1324. doi: https://doi.org/10.1002/2016JC012437

Witek, M. L., Teixeira, J., & Matheou, G. (2011a). An Eddy Diffusivity–Mass Flux Approach to the Vertical Transport of Turbulent Kinetic Energy in Convective Boundary Layers. *J. Atmos. Sci.*, *68*(10), 2385–2394. doi: 10.1175/JAS-D-11-06.1

Witek, M. L., Teixeira, J., & Matheou, G. (2011b). An Integrated TKE-Based Eddy Diffusivity/Mass Flux Boundary Layer Closure for the Dry Convective Boundary Layer. *J. Atmos. Sci.*, *68*(7), 1526–1540. doi: 10.1175/2011JAS3548.1

Wu, X., & Yanai, M. (1994). Effects of Vertical Wind Shear on the Cumu-

lus Transport of Momentum: Observations and Parameterization. *J. Atmos. Sci.*, *51*(12), 1640–1660. doi: 10.1175/1520-0469(1994)051⟨1640:EOVWSO⟩2.0.CO;2

Wyngaard, J. C., & Coté, O. R. (1971). The Budgets of Turbulent Kinetic Energy and Temperature Variance in the Atmospheric Surface Layer. *J. Atmos. Sci.*, *28*(2), 190–201. doi: 10.1175/1520-0469(1971)028⟨0190:TBOTKE⟩2.0.CO;2

Yano, J.-I. (2014). Formulation structure of the mass-flux convection parameterization. *Dynam. Atmos. Oceans*, *67*, 1–28. doi: 10.1016/j.dynatmoce.2014.04.002

Young, W. R. (2010). Dynamic Enthalpy, Conservative Temperature, and the Seawater Boussinesq Approximation. *J. Phys. Oceanogr.*, *40*(2), 394–400. doi: 10.1175/2009JPO4294.1

Zhang, M., Somerville, R. C. J., & Xie, S. (2016, April). The SCM Concept and Creation of ARM Forcing Datasets. *Meteorol. Monogr.*, *57*(1), 24.1–24.12. doi: 10.1175/AMSMONOGRAPHS-D-15-0040.1

Zheng, Z., Harcourt, R. R., & D'Asaro, E. A. (2021). Evaluating Monin–Obukhov Scaling in the Unstable Oceanic Surface Layer. *J. Phys. Oceanogr.*, *51*(3), 911–930. doi: 10.1175/JPO-D-20-0201.1